Feasibility Study of Exotic Particle X(3872) with ATHENA in EIC Experiment and its Possible Structures

M.Sc. Thesis

By

Diksha Sharma

Department of Physics
Indian Institute of Technology Indore

June 2022

Feasibility Study of Exotic Particle X(3872) with ATHENA in EIC Experiment and its Possible Structures

A Thesis

Submitted in partial fulfillment of the requirements for the award of the degree

of

Master of Science

By

Diksha Sharma

Department of Physics
Indian Institute of Technology Indore

June 2022

Indian Institute of Technology Indore

Candidate's Declaration

I hereby certify that the work which is being presented in the thesis entitled **Feasibility Study of Exotic Particle X(3872) with ATHENA in EIC Experiment and its Possible Structures** in the partial fulfillment of the requirements for the award of the degree of **Master of Science** and submitted in the **Department of Physics, Indian Institute of Technology Indore**, is an authentic record of my work carried out during the time period from July 2021 to June 2022 under the supervision of **Dr. Ankhi Roy, Associate professor, Indian Institute of Technology Indore.**

The matter presented in the thesis has not been submitted by me for the award of any other degree at this or any institute.

Diksha
31/05/22
Signature of student with date
(Diksha Sharma)

This is to certify that the above statement made by the candidate is correct to the best of my knowledge.

Ankhi Roy **04/06/2022**
Signature of the Supervisor of
M.Sc. thesis (with date)
(**Dr. Ankhi Roy**)

Diksha Sharma has successfully given her M.Sc. thesis.

Ankhi Roy
Signature of supervisor of MSc thesis
(Dr. Ankhi Roy)
Date: **04/06/2022**

Signature of convener, DPGC
Date: 07/06/2022

Subhendu Rakshit
Signature of PSPC member
(Prof. Subhendu Rakshit)
Date: 04.06.2022

Sarkar
Signature of PSPC member
(Dr. Debajyoti Sarkar)
Date: 06/06/22

Abstract

The normal hadrons known as protons, neutrons, pions, etc are classified according to the quark model but there are some other particles named exotic particles that can not be classified by the quark model but are favored by Quantum Chromodynamics (QCD). Some of these particles contain heavy quarks and have different quark compositions than normal hadrons like four quarks, five quarks, gluonic degrees of freedom, and gluon-gluon interactions. A feasibility study of exotic particles has been done in the future Electron-Ion Collider (EIC) experiment with a totally hermetic electron nucleus apparatus (ATHENA) detector concept. A phenomenological approach for understanding exotic particles in quark-gluon plasma (QGP) medium with a multiphase transport model (AMPT) has been done.

Acknowledgements

First and foremost, I'd like to express my gratitude to Dr. Ankhi Roy, my supervisor, without whose direction and unwavering support it would have been difficult for me to have a deeper understanding of the subject. Working under her for my thesis has been a tremendous honor, and it goes without saying how much her knowledge, supervision, and support have aided my development, not only academically but also personally. She, as a mentor, provided essential advice and bolstered my spirits anytime I encountered adversity, and I will be eternally grateful.

I am thankful to Prof. Subhendu Rakshit & Dr. Debajyoti Sarkar for being my PSPC committee members. I am immensely thankful to the entire faculty of the Department of Physics at IIT Indore for all the courses which I have been taught during my degree and for conducting my seminar in such a smooth and efficient manner.

I am thankful to Justin Stevens from Jeffersons lab, Dr. Neha Shah from IIT Patna, and Dr. Amal Sarkar from Calcutta University for their guidance during the ATHENA meeting in collaboration. I am thankful to Hridey Chetri for helping me in EIC work.

I am extremely thankful to all of my lab seniors for their encouragement and invaluable assistance. I am thankful to Yoshini for guiding me. I am also grateful to all of my closest friends, especially Kanika, Kailash, and Nilay for assisting me in achieving the much-needed work-life balance.

Last but not least, I want to express my gratitude to my parents for allowing me to pursue my dreams and objectives while also guiding me in every part of my life. This thesis is a dedication to all I've learned about life through my family, friends, instructors, and supervisors, as well as a tribute to the enormous amount of effort I've put into it.

Contents

List of Figures

Chapter 1

Introduction

Nature is made up of matter and matter is made of particles. First elementary charge particle electron was discovered by J.J. Thomson in 1897, then proton was discovered by Rutherford and then in 1932 neutron was discovered by Chadwick. From that period of time to till now many particles were discovered and categorized. There are matter particles and mediators. The matter particles are divided into two types: hadrons and leptons. The leptons are elementary particles and hadrons are particles that are made up of elementary particles called quarks. Every particle has its antiparticle which has the same mass, spin, and isospin as the particle but opposite quantum numbers [1]. All the elementary particles are shown in Figure 1.1.

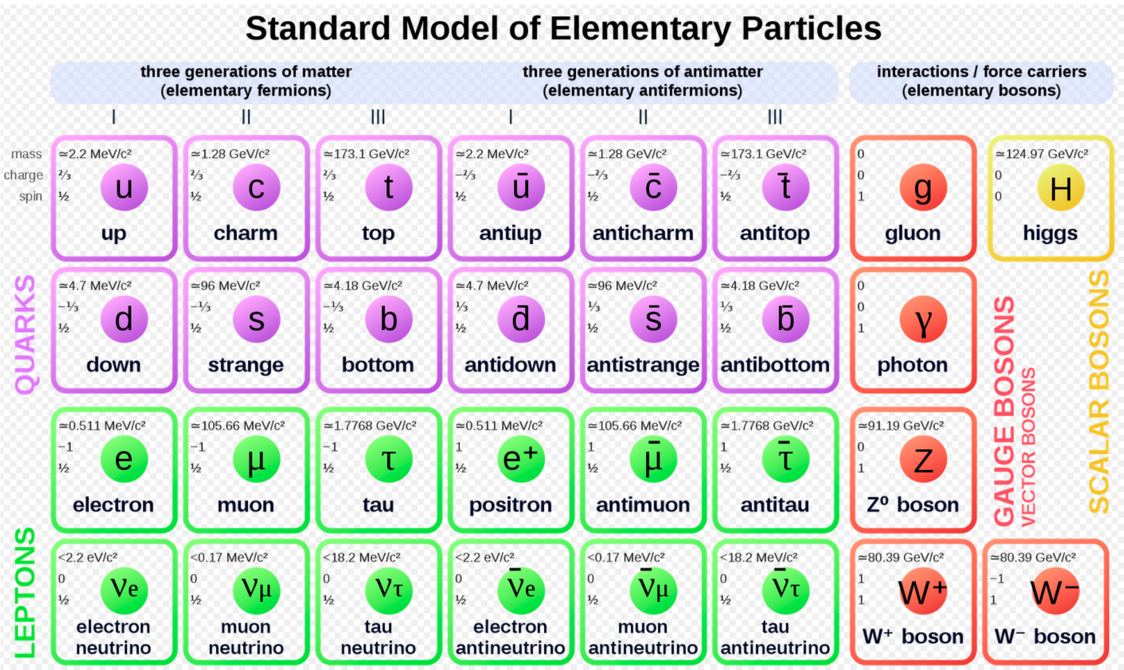

Figure 1.1: Different elementary particles and antiparticles with their mass, charge, and spin.

The quark model [1] which was formulated in 1964 has two composition rules for hadrons:

1. Baryon is composed of three quarks.

2. Meson is composed of a quark and antiquark.

In the universe, there are four fundamental forces: electromagnetic, strong, weak, and gravitational. As the name suggests, of all these forces strong force is the strongest. Its range is of the order 10^{-15} m (1 fm). It confines quarks into hadrons such as protons and neutrons. The mediator of the strong force is gluon which transfers the force between quarks. Unlike photons which are a mediator of the electromagnetic interaction and do not carry the charge, the gluon carries color (blue, red, and green). The gluons are bicolored and can interact with each other. The theory that describes strong interaction is quantum chromodynamics (QCD) [1]. It is based on the SU(3) gauge symmetry group and its quantum number is color. In the standard model, hadrons are described by QCD. QCD has two properties: asymptotic freedom and color confinement. Asymptotic freedom implies that interactions between particles become asymptotically weaker as the energy scale increases and the corresponding length scale decreases. Color confinement implies that every particle should be color neutral. This property of QCD allows more complicated structures like tetraquark, pentaquark, etc.

In this chapter, we will first discuss about exotic particles, their naming, and possible structures. Then we will discuss about exotic particle X(3872) and related work using it. Let us discuss this in detail.

1.1 Exotic Particles

For a long time, hadrons have been classified as mesons $q\bar{q}$ and baryons qqq but as the color neutrality of particles holds there are more possibilities other than these hadrons. So, the particles other than these hadrons whose quantum number does not fit in the quark model are known as exotic particles. In 2003, the first exotic particle was discovered named as X(3872) by the Belle experiment [3]. After this many more particles were discovered. In Table 1.1, some of the exotic particles are quoted which were discovered in the given experiment and decay channel with their experimentally observed quantum numbers [3].

1.1.1 Naming of Exotic Particles

The meson made of a heavy quark and antiquark pair is called quarkonia. The charmonium ($\bar{c}c$ quarkonia) and the bottomonium ($\bar{b}b$ quarkonia) fit within the

Table 1.1: Exotic particles with the experiment, decay channel and experimentally calculated quantum numbers, J^{PC}.

Particle	Experiment : Decay Channel	J^{PC}
X(3872)	BELLE: $B \to K\pi^+\pi^- J/\psi$	1^{++}
$\chi_{c0}(3860)$	BELLE: $e^+e^- \to J/\psi D\bar{D}$	0^{++}
$\chi_{c1}(4140)$	CDF Collaboration: $B^+ \to \chi_{c1}K^+, \chi_{c1} \to \phi J/\psi$	1^{++}
$\chi_{c1}(4274)$	LHCb: $B^+ \to \phi J/\psi K^+, \chi_{c1} \to \phi J/\psi$	1^{++}
Y(4260)	BaBar: $e^+e^- \to \pi^+\pi^- J/\psi$	1^{--}
Y(4230)	BESIII: $e^+e^- \to \pi^+\pi^- J/\psi$	1^{--}
$\psi(4360)$	BaBar: $e^+e^- \to \pi^+\pi^- \psi(2S)$	1^{--}
$\psi(4660)$	BELLE: $e^+e^- \to \pi^+\pi^- \psi(2S)$	1^{--}
$Z_c(3900)$	BESIII: $e^+e^- \to \pi^+\pi^- J/\psi$	1^{+-}
$Z_b(10610)$	BELLE: $\Upsilon(5S) \to \Upsilon(nS)\pi^+\pi^-, n = 1, 2, 3$	1^{+-}
$Z_b(10650)$	BELLE: $\Upsilon(5S) \to \pi^+\pi^- h_b(mP), m = 1, 2$	1^{+-}

quark model. Many hadrons were found containing a heavy quark and antiquark, but with properties not matching with those expected for ordinary quarkonia so they are named as exotic particles or quarkonium like states.

These exotic particles were known as XYZ states as they were named either X(mass), or Y(mass), or Z(mass) by experimental collaborations. The states whose quantum numbers are not yet fixed are named as X(mass), for example X(3915), X(3860), etc. The states which have quantum number J^{PC}=1^{--} are named as Y(mass), for example Y(4360), Y(4660), etc. The states with isospin 1 and quantum number J^{PC}=1^{+-} containing a $c\bar{c}$ pair and $b\bar{b}$ pair are named as Z_c(mass) and Z_b(mass), respectively, for example Z_c(4430).

Particle Data Group (PDG) has proposed a new naming scheme for these particles as shown in Table 1.2. Naming is done for example: a state containing a $\bar{c}c$ pair with the quantum numbers 1^{-+} is called η_{c1}. Similarly, other states can be named like states containing $c\bar{c}$ with J=2 or quantum number 2^{++} as χ_{c2} [2].

Table 1.2: Naming scheme of quarkonium and quarkonium like states by PDG.

	PC	$-+$	$+-$	$--$	$++$
Isospin	heavy quark content				
I = 0	with $c\bar{c}$	η_c	h_c	ψ	χ_c
I = 0	with $b\bar{b}$	η_b	h_b	Υ	χ_b
I = 1	with $c\bar{c}$	Π_c	Z_c	R_c	W_c
I = 1	with $b\bar{b}$	Π_b	Z_b	R_b	W_b

The exotic particles like X(3872), $\psi(4040)$ etc lie in charmonium spectrum as shown in Figure 1.2 and Y(2S), Y(3S) etc lie in bottomonium spectrum as shown in Figure 1.3 [2]. Spectrum implies that the exotic particles contain those heavy quarks and antiquarks. For exotic particles lie in charmonium states, dashed lines show some thresholds that are open in the that mass range, here D_1 stands for $D_1(2420)$ and D_2^* for $D_2^*(2460)$. The states shown to the right in the two columns are isovectors containing a $\bar{c}c$ pair; they are exotic particles. All states below the lowest open-flavor threshold ($\bar{D}D$) are normal states. Similarly, for bottomonium states, dashed lines show the open-bottom thresholds $\bar{B}B$, $\bar{B}B^*$, $\bar{B}^*B^*$, $\bar{B}B_1(5721)$, $\bar{B}B_2^*(5747)$, $\bar{B}^*B_1(5721)$, and $\bar{B}^*B(5747)$.

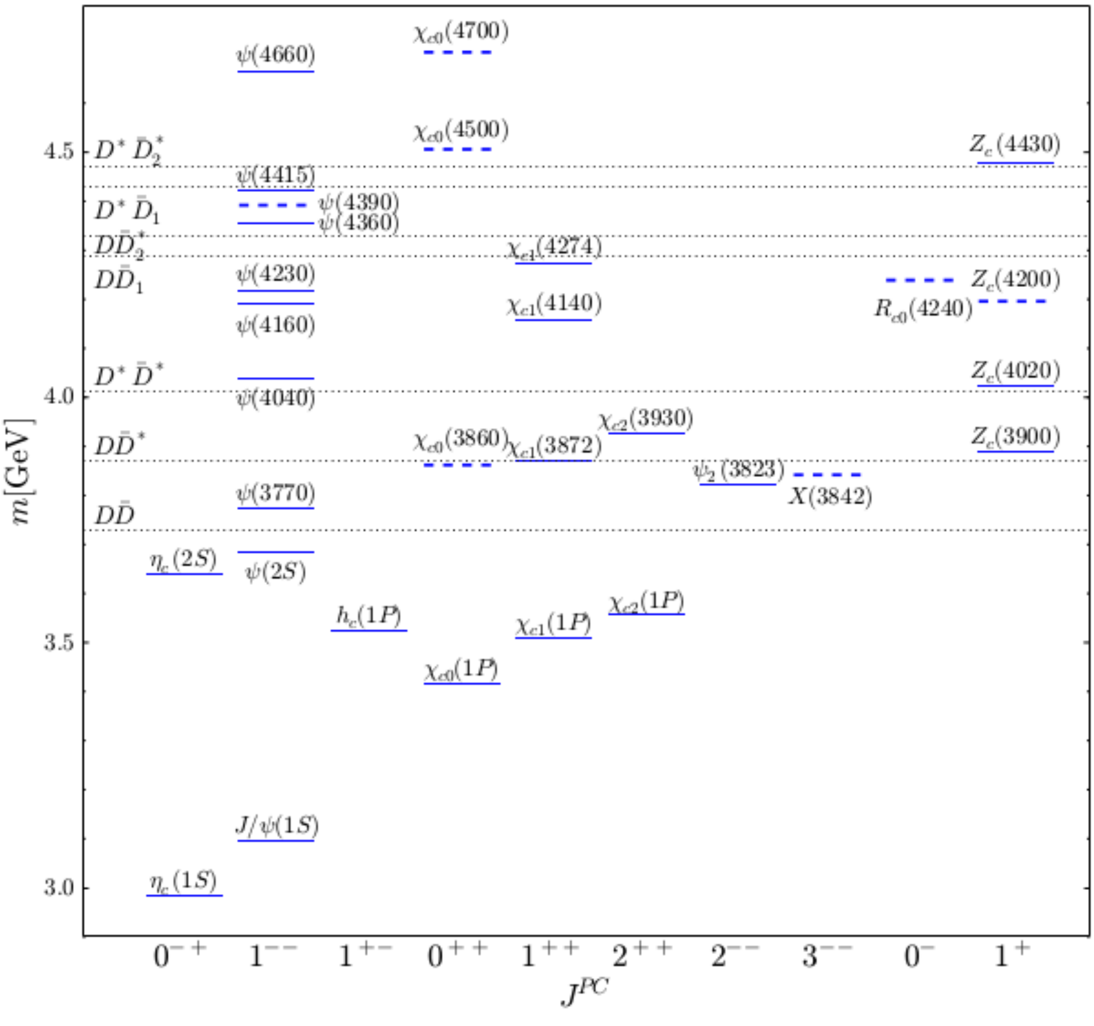

Figure 1.2: Charmonium spectrum of particles with their mass threshold and quantum numbers.

1.1.2 Possible Structures of Exotic Particles

The exotic particles can have different types of structure depending on the presence of active gluons. They can be classified as shown in Figure 1.4 [2].

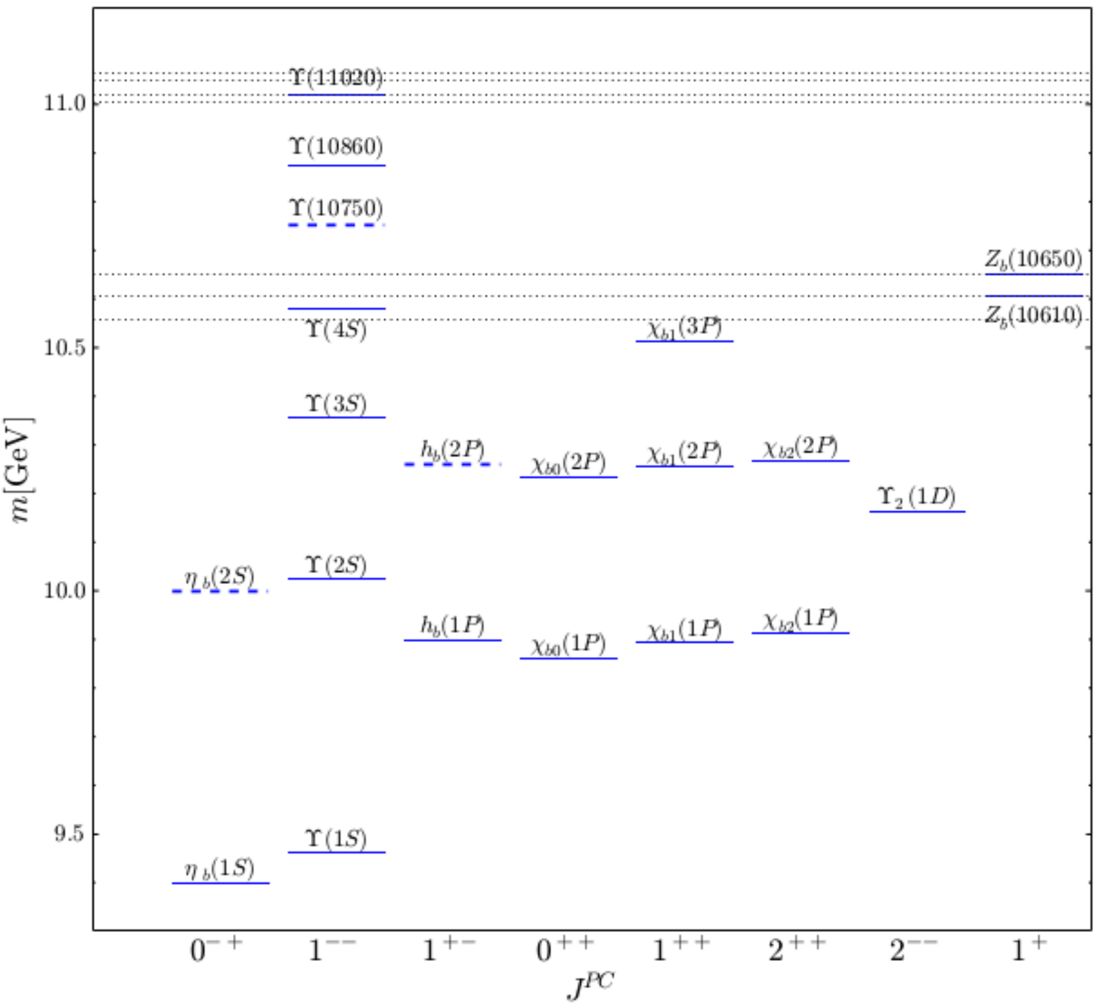

Figure 1.3: Bottomonium spectrum of particles with their mass threshold and quantum numbers.

Multiquark Configurations

1. Compact Tetraquark: It is a multi quark state containing $\bar{Q}\bar{q}$ and Qq where Q denoted heavy quark and q denotes light quark. Here, the spin-spin interaction is operative inside the diquarks not between the light quarks. Its possible candidates are X(3872), $Z_b(10610)$ etc.

2. Hadroquarkonium: It consists of heavy quark-antiquark to form a compact core that is surrounded by light quark clouds. In the decay, the compact core remains intact while the light quark cloud comes out in terms of multipion states. The core and cloud are held together by the QCD analogue of Van der waals force. Its possible candidates are $Z_c(4100)$, $Z_c(4200)$ etc.

3. Hadronic Molecule: It is made up of hadrons. X(3872), $Z_c(3900)$ and Y(4360) in the charmonium state and $Z_b(10610)$ and $Z_b(10650)$ in the bottomonium state are good candidates for having hadronic molecule structure.

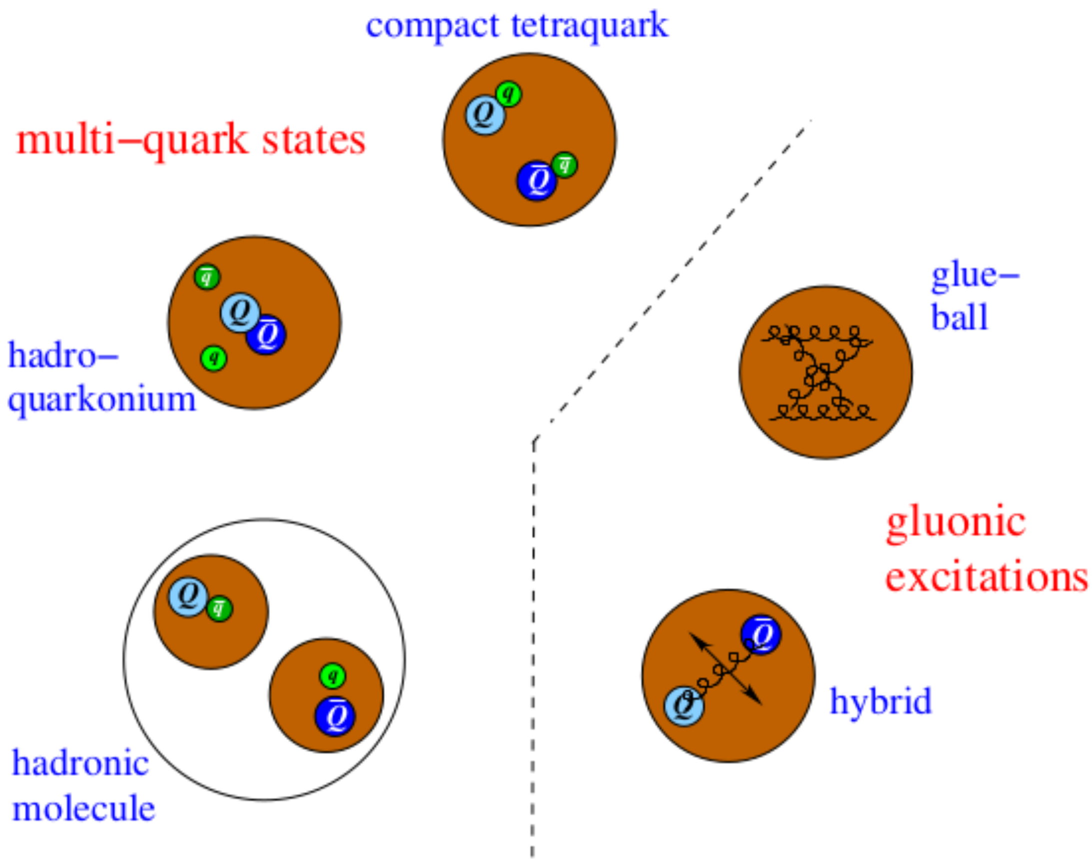

Figure 1.4: Different structures of exotic particles.

Based on Gluonic Excitations

1. Hybrids: It contains quark-antiquark pairs with one or more active gluons. The excitation of the gluonic degrees of freedom contributes at least with approximately 1 GeV/c^2 to the mass of the system. Its possible candidate is Y(4230).

2. Glueballs: It contains gluon-gluon pairs. Many searches have been made till now but there is no experimental confirmation of its existence till now.

1.2 Exotic Particle: X(3872)

As we are interested to study exotic particles and for this, the X(3872) is the most studied prime example to work on. X(3872) was observed in the $\pi\pi J/\psi$ final state in the Belle experiment whose properties do not match with ordinary hadrons which contain charm and anti charm pair for sure. X(3872) was first observed in $B \to K\pi^+\pi^- J/\psi$ decays as a narrow peak in the invariant mass distribution of the $\pi^+\pi^- J/\psi(1S)$ final state. Later on, its existence was confirmed by many other experiments. its quantum number $J^{PC} = 1^{++}$ was confirmed by the LHCb experiment [5] in 2013.

To know the structure of X(3872) many researches are going on. It can have either a hadronic molecule type of structure or tetraquark type of structure (as shown in Figure 1.5) [6]. Its proximity to the ($D\bar{D}^*+$ charge conjugate) mass threshold indicates its hadronic molecular picture. The molecular state can be made by the coalescence of two charmed mesons. There are also other scenarios, such as diquark-antidiquark tetraquark, hybrid, charmonium, the quantum mixture of $\chi_{c1}(2P)$ and $D^0\bar{D}^{*0}$, as well as other configurations.

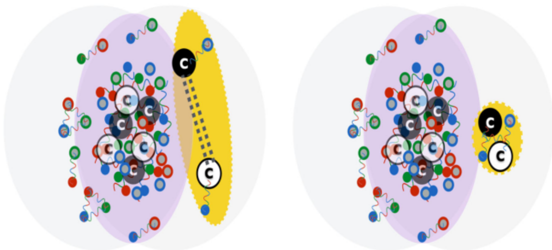

Figure 1.5: Illustration of X(3872) structure as molecular (left) and tetraquark (right).

1.3 Electron Ion Collider (EIC) Experiment

The EIC [4] will be a new collider facility capable of revolutionizing our knowledge of QCD in the next decades. The EIC is envisioned as a premier facility to study the structure and dynamics of visible matter. It is a new large-scale particle accelerator facility conceived by U.S. nuclear and accelerator physicists. The EIC will study protons, neutrons and atomic nuclei with the most powerful electron microscope, in terms of resolving power and intensity, ever built. The EIC will be a discovery machine for unlocking the secrets of the "glue" that binds the building blocks of visible matter in the universe.

In EIC, they will collide electron-proton, electron-nucleus, and nuclei-nucleus. The EIC will be the world's first polarized electron-proton collider—meaning the spins of both colliding particles can be aligned in a controlled way. This will make it possible to experimentally solve the outstanding mystery of how the teeming quarks and gluons inside the proton combine their spins to generate the overall spin carried by the proton. Experiments at the EIC will offer novel insight into why quarks or gluons can never be observed in isolation but must transform into and remain

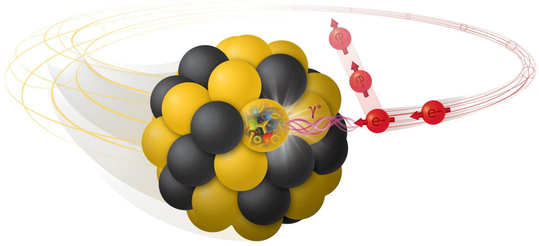

Figure 1.6: visualization of electron-nucleus collision at EIC.

confined within protons and nucleus. The EIC with its unique combinations of high beam energies and intensities will cast fresh light into the quark and gluon confinement, a key puzzle in the Standard Model of physics.

In this thesis, using X(3872), a feasibility study in EIC experiment and phenomenological study to know its structure will be discussed.

The feasibility study is done by physics simulation of exotic particles with EIC experiment which will happen in future in which they are doing a different kind of $e^{-}p$ and $e^{-}A$ collisions (where A stands for different nucleus) which produces different nuclear medium which may help to reveal the structure of exotic particles. The feasibility study is done to know whether the exotic particles will be detected in an EIC environment or not. Also, whether different nuclear mediums can help in knowing the structure of exotic particles or not.

Relativistic heavy ion collision which produces QGP medium can be a good experiment to study the structure of exotic particles. The study of the structure of exotic particles is done using heavy ion collision through an AMPT event generator which is a Monte Carlo framework.

Chapter 2

Analysis Tools

In this chapter, we will first discuss about the different observables used to study the exotic particles then about ATHENA detector, and software like ROOT, and AMPT to fulfill our physics goals will be discussed.

2.1 Observables

The observables used for the study of exotic particles are as follows:

- Transverse momentum (p_T) : It is the component of momentum perpendicular to the beam line. its unit is GeV/c. Let's say beam line is z axis or longitudinal momentum is p_z as shown in Figure 2.1 then transverse momentum (p_T) is given by

$$p_T = \sqrt{p_x^2 + p_y^2} \tag{2.1}$$

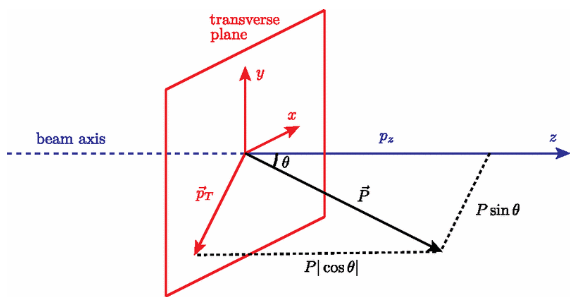

Figure 2.1: Standard geometry of collider experiment.

- Rapidity (y) : It is the relativistic analogue of velocity. It is given by

$$y = tanh^{-1}\beta = \frac{1}{2}ln\frac{1+\beta}{1-\beta} = \frac{1}{2}ln\frac{E+p_z}{E-p_z} \tag{2.2}$$

where β = p_z/E and p_z is longitudinal momentum. Rapidity of the particle in one frame of reference is related to the rapidity in another Lorentz frame of reference by an additive constant. The difference between rapidities of two colliding particles is invariant with respect to Lorentz boost along the z axis.

- Pseudorapidity (η) : At very high energy, $p \gg m$, rapidity can be written as

$$y = -ln\left(tan\frac{\theta}{2}\right) = \eta \tag{2.3}$$

where θ is the polar angle or particle production angle measured with respect to the beamline in experiments and η is called pseudorapidity. For highly relativistic particles, it is hard to measure the energy and momentum of a particle but easier to measure the angle of the detected particle i.e. θ relative to the beam axis (z). η is defined for any value of momentum, energy, and mass of a particle. As shown in Figure 2.2, as the polar angle increases pseudorapidity decreases. The forward direction in experiments is at high $|\eta|$.

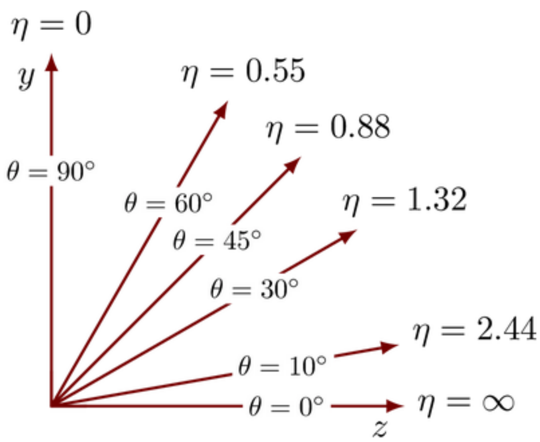

Figure 2.2: Pseudorapidity as a function of polar angle.

- Elliptic flow (v_2) : It also describes the azimuthal momentum space anisotropy of particle emission for heavy ion collisions in transverse plane to beam line [7].
It is given by second harmonic coefficient of azimuthal distribution of particle emission which is analyzed with respect to reaction plane that is

$$v_2 = \langle cos2(\phi - \phi_r)\rangle \tag{2.4}$$

where ϕ is azimuthal angle of particle and ϕ_r is azimuthal angle of reaction

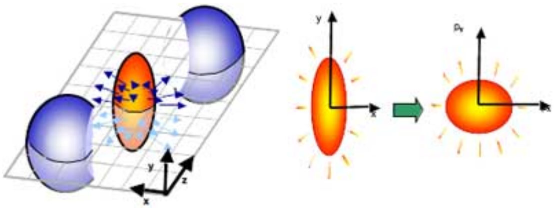

Figure 2.3: Left: Schematic of the collision zone between two incoming nucleus and x-z is the reaction plane. Right: Initial-state anisotropy in the collision zone converting into final-state elliptic flow, measured as anisotropy in particle momentum.

plane in lab frame given by

$$\phi_{\mathrm{r}} = \frac{1}{2}\left(\tan^{-1}\frac{\Sigma_{\mathrm{i}}\mathrm{w}_{\mathrm{i}}\sin(2\phi_{\mathrm{i}})}{\Sigma_{\mathrm{i}}\mathrm{w}_{\mathrm{i}}\sin(2\phi_{\mathrm{i}})}\right) \tag{2.5}$$

For v_2, w_i is weight factor equal to p_T. Space to momentum anisotropy is visualised in Figure 2.3.

- Efficiency of Particle Detection: It is given by:

$$\text{Efficiency} = \frac{\text{Number of reconstructed particles}}{\text{Number of generated particles}} \times 100\,\% \tag{2.6}$$

Here, generated particles are those which are generated from collision and reconstructed particles are those which are reconstructed back from decay particles. While calculating efficiency, the errors per bin are calculated as the square root of the sum of squares of weights for each bin using an inbuilt function in ROOT that is Sumw2.

- Mass resolution: The particles have some particular mass which is detected by its decay channel and using a detector it is reconstructed by its invariant mass. Due to the limitations of the detector a distribution of mass is obtained in spite of a spike at one value. So, the difference in mass of reconstructed particles and generated particles is taken and then fit it with some distribution which is Gaussian in our case to obtain the resolution of the particle. It basically helps us to know the resolution of the detector. To obtain the mass resolution, the mass difference (reconstructed mass-generated mass) is fitted using double Gaussian fitting. For the fitting, two Gaussian functions are taken and add them to find the final Gaussian function, and taking parameters from the final Gaussian two Gaussian functions are plotted.

2.2 ATHENA Detector

A totally hermetic electron nucleus apparatus (ATHENA) [9] is a proposed detector for the future EIC experiment, in Brookhaven National Laboratory, United States. It is providing the best possible acceptance, resolution, and particle identification capabilities and is designed for Interaction Point 6 (IP6) to deliver the full physics program at EIC. The ATHENA detector is a hermite detector that can fire parti-

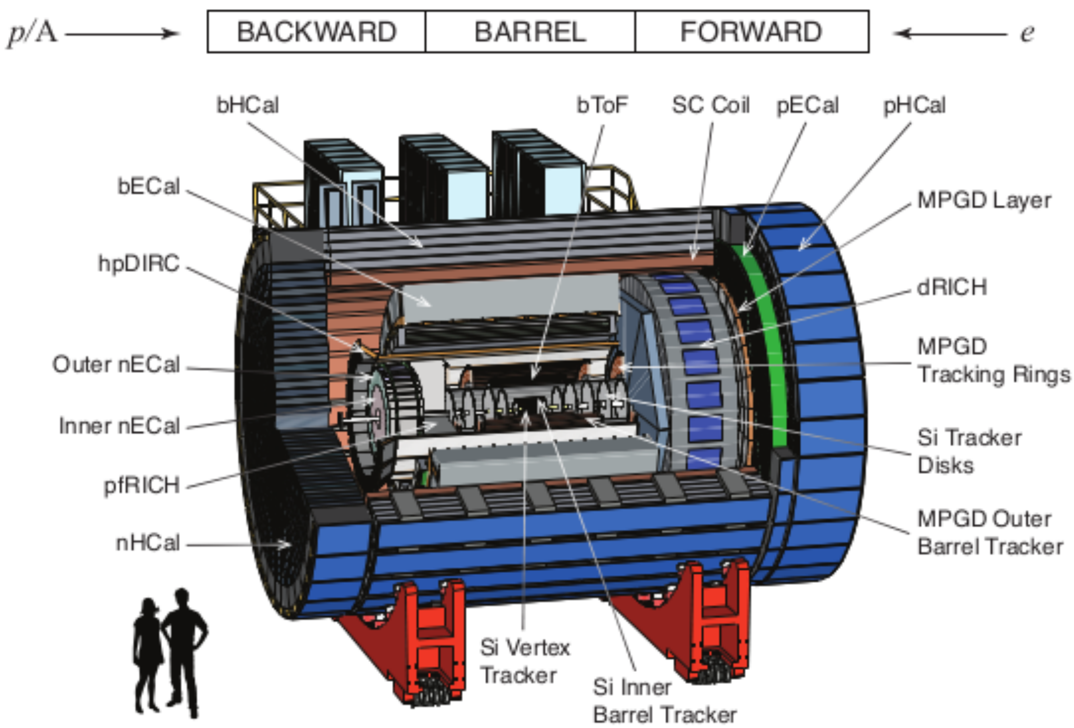

Figure 2.4: Open view of ATHENA detector. The detector acronyms are given in glossary.

cles from both forward and backward regions. The integrated ATHENA detector is shown in Figure 2.4. It can be seen that protons or nuclei will be fired from the backward region and electrons will be fired from the forward region. The detector consists of an inner tracking system (vertex layers, barrel layers, and disks) based on silicon Monolithic Active Pixel Sensors (MAPS) technology complemented by cylindrical Micro mesh Gas Detector (Micromegas) layers at larger radii in the barrel and Gas Electron Multiplier (GEM) rings in the forward/backward direction. A high-performance DIRC (hpDIRC) detector in the barrel, a dual radiator RICH (dRICH) in the forward region, and a single-volume proximity-focusing RICH (pfRICH) in the electron, endcap is fixed for particle identification. To improve tracking and pointing accuracy, a micro-Resistive Well (μRWell) tracker is positioned behind the dRICH in the forward region. In the imaging part of the barrel Electromagnetic Calorimeter (bECal), tracking information in the barrel region is provided.

The forward calorimeters contain a W/SciFi electromagnetic calorimeter (pECal) augmented by an iron-scintillator sampling hadronic calorimeter (pHCal).

2.2.1 ATHENA Software

The ATHENA singularity container [10] holds the "eic-shell" which contains all the necessary software required for the construction, simulation, visualization, etc of the detector as well as particle reconstruction and analysis. ROOT, Pythia8, HEPMC, Gaudi, and more software are included in the container. DD4hep is a software framework included in the singularity container for providing a complete solution to full detector description (geometry, materials, visualization, readout, alignment, calibration, etc.) for the full experiment life cycle which includes detector concept development, detector optimization, construction, operation.
For generating data elSpectro event generator is used which is a framework for incorporating spectroscopy into electro/photoproduction reactions.

2.3 ROOT

ROOT [8] is a framework used in experimental high energy physics. It is an object-oriented program and library which is developed by CERN. It was designed for particle physics data analysis as it contains several features specific to this field, but it is also used in other applications such as astronomy and data mining. It is a data analysis framework that helps in histogramming, fitting, statistical analysis, and in storing large collision events. It is designed for high computing efficiency.

2.4 A Multiphase Transport Model (AMPT)

AMPT [11] is a Monte Carlo transport model for heavy ion collisions at relativistic energies. It includes both initial and final hadronic interactions and the transition between these two phases of matter. It is developed to describe nuclear collisions ranging from p + A to A + A systems at center-of-mass energies from about $\sqrt{s_{NN}}$ = 5 GeV up to 5500 GeV at LHC.

The AMPT model consists of four main stages: the initial conditions, partonic interactions, the conversion from the partonic to the hadronic matter, and hadronic interactions. It aims to provide a kinetic description of all these essential stages of heavy ion collisions.

It is available in two versions default and string melting whose structures are shown in Figure 2.5 and 2.6 respectively. The full source code of the AMPT model in the Fortran 77 language and instructions for users are available online at the OSCAR website and also at the EPAPS website. The default AMPT model is named as version 1.x, and the AMPT model with string melting is named as version 2.y, where value of the integer extension x or y increases whenever the source code is modified.

The initial conditions in the AMPT model are obtained using the Heavy Ion Jet

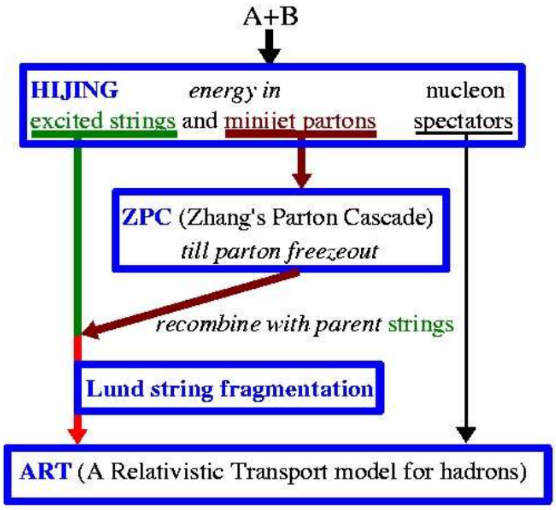

Figure 2.5: Structure of default AMPT model.

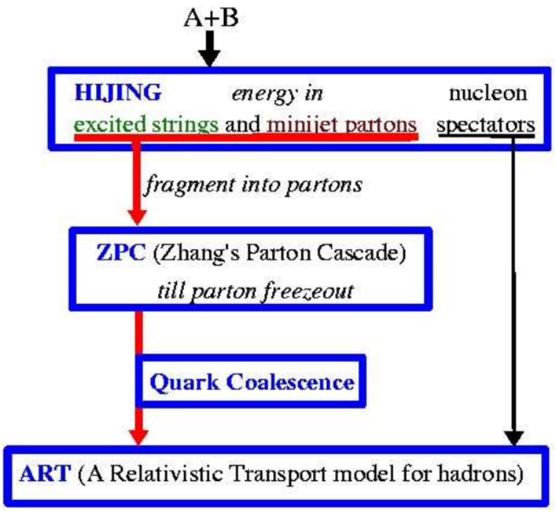

Figure 2.6: Structure of default AMPT model.

Interaction Generator (HIJING) model. In the HIJING model, the particles produced from the collision of two nucleons are described in terms of a hard and a soft component. The hard component processes are those in which the momentum transfer is larger than a cutoff momentum p_0. These hard processes produce energetic minijet partons. The soft component processes are those in which momentum transfer is below p_0 and is modeled by the formation of strings. The partonic part in the default AMPT model includes only minijets. And string melting includes all excited strings that are not projectile and target nucleons without any interactions. Scatterings among the partons are described by Zhang's Parton Cascade (ZPC) which includes only two-body scatterings with cross sections obtained from the pQCD with screening masses. For conversion from the partonic to the hadronic matter, the default AMPT model uses the Lund string fragmentation model and the string melting model uses the quark coalescence model. According to the Lund string fragmentation model, after minijet partons stop interacting, they are combined with their parent strings to form excited strings, which are then converted to hadrons. And in the quark coalescence model, the two nearest partons combine into a meson and the three nearest quarks (antiquarks) into a baryon (antibaryon). The Hadron cascade in the AMPT model is based on the A Relativistic Transport Model (ART) developed for heavy ion collisions. The ART model includes baryon-baryon, baryon-meson, and meson-meson elastic and inelastic scatterings. It treats explicitly the isospin degrees of freedom for most particle species and their interactions, making it suitable for studying isospin effects in heavy ion collisions. It includes secondary interactions for π, ρ, ω, η, K, K^*, ϕ, Δ, $N^*(1440)$ etc.

To run the AMPT program, the initial parameters needed to be set in input.ampt as shown in Figure 2.7. If preferred that every run is different even with the same 'input.ampt' file, use 'ihjsed=11'. And to execute the file, type 'sh exec &' to compile and run, it executes 'ampt' with some general information written in 'nohup.out'.

Key output files are 'ampt.dat' and 'zpc.dat. 'ampt.dat' contains particle records at hadron kinetic freeze-out. For each event, the first line gives the event number, test number (=1), number of particles in the event, impact parameter, total number of participant nucleons in the projectile, the total number of participant nucleons in target, number of participant nucleons in projectile due to elastic collisions, number of participant nucleons in projectile due to inelastic collisions, and corresponding numbers in the target. Note that participant nucleon numbers include nucleons participating in both elastic and inelastic collisions. Each of the following lines gives: PYTHIA particle ID number, three-momentum (p_x, p_y, p_z), mass, and space-time coordinates (x, y, z, t) of one final particle at freeze-out.

zpc.dat is similar to 'ana/ampt.dat' but for partons. The first line of each event gives the event number, number of partons in the event, impact parameter, number of participant nucleons in projectile due to elastic collisions, the number of participant

```
2760            ! EFRM (sqrt(S_NN) in GeV if FRAME is CMS)
CMS             ! FRAME
A               ! PROJ
A               ! TARG
208             ! IAP (projectile A number)
82              ! IZP (projectile Z number)
208             ! IAT (target A number)
82              ! IZT (target Z number)
200000          ! NEVNT (total number of events)
9.8             ! BMIN (mininum impact parameter in fm)
9.8             ! BMAX (maximum impact parameter in fm, also see below)
4               ! ISOFT (D=4): select Default AMPT or String Melting(see below)
150             ! NTMAX: number of timesteps (D=150), see below
0.2             ! DT: timestep in fm (hadron cascade time= DT*NTMAX) (D=0.2)
2.2             ! PARJ(41): parameter a in Lund symmetric splitting function
0.5             ! PARJ(42): parameter b in Lund symmetric splitting function
1               ! (D=1,yes;0,no) flag for popcorn mechanism(netbaryon stopping)
1.0             ! PARJ(5) to control BMBbar vs BBbar in popcorn (D=1.0)
1               ! shadowing flag (Default=1,yes; 0,no)
0               ! quenching flag (D=0,no; 1,yes)
2.0             ! quenching parameter -dE/dx (GeV/fm) in case quenching flag=1
2.0             ! p0 cutoff in HIJING for minijet productions (D=2.0)
1.8d0           ! parton screening mass in fm^(-1) (D=2.265d0), see below
0               ! IZPC: (D=0 forward-angle parton scatterings; 100,isotropic)
0.47d0          ! alpha in parton cascade (D=0.33d0), see parton screening mass
1d6             ! dpcoal in GeV
1d6             ! drcoal in fm
0               ! ihjsed: take HIJING seed from below (D=0)or at runtime(11)
13150909        ! random seed for HIJING
8               ! random seed for parton cascade
0               ! flag for K0s weak decays (D=0,no; 1,yes)
1               ! flag for phi decays at end of hadron cascade (D=1,yes; 0,no)
0               ! flag for pi0 decays at end of hadron cascade (D=0,no; 1,yes)
0               ! optional OSCAR output (D=0,no; 1,yes; 2&3,more parton info)
0               ! flag for perturbative deuteron calculation (D=0,no; 1or2,yes)
1               ! integer factor for perturbative deuterons(>=1 & <=10000)
1               ! choice of cross section assumptions for deuteron reactions
-7.             ! Pt in GeV: generate events with >=1 minijet above this value
1000            ! maxmiss (D=1000): maximum # of tries to repeat a HIJING event
3               ! flag on initial and final state radiation (D=3,both yes; 0,no)
1               ! flag on Kt kick (D=1,yes; 0,no)
0               ! flag to turn on quark pair embedding (D=0,no; 1,yes)
7., 0.          ! Initial Px and Py values (GeV) of the embedded quark (u or d)
0., 0.          ! Initial x & y values (fm) of the embedded back-to-back q/qbar
1, 5., 0.       ! nsembd(D=0), psembd (in GeV),tmaxembd (in radian).
0               ! Flag to enable users to modify shadowing (D=0,no; 1,yes)
1.d0            ! Factor used to modify nuclear shadowing
0               ! Flag for random orientation of reaction plane (D=0,no; 1,yes)
```

Figure 2.7: Input file for AMPT.

nucleons in projectile due to inelastic collisions, and corresponding numbers in the target. Each of the fol- lowing lines give PYTHIA particle ID number, three-momentum (p_x, p_y, p_z), mass, and space-time coordinates (x, y, z, t) of one final parton at freeze- out.

Now let us study the exotic particles using these analysis tools in detail.

Chapter 3

Physics Simulation of X(3872)

The feasibility study is done by physics simulation of X(3872) with ATHENA software. In the feasibility study, kinematic distributions, the efficiency of identified particles, and mass resolution of particles decayed from X(3872) are done. The kinematic distributions can give an idea about the detector's geometry as the distribution of decay particles can be computed from it. The efficiency of identified decay particles can give an idea about how effective the detector is in detecting particles and mass resolution tells whether the particle which is reconstructed is the same particle or not.

3.1 Framework

To study the exotic particle X(3872), the physics simulation of X(3872) is done using ATHENA software.

3.1.1 Data & Selection Procedure

1. elSpectro event generator is used to generate exotic particle data that is used for study.
2. The decay channel is
   $e^-p \to X(3872) \to J/\psi\pi^+\pi^-, J/\psi \to e^+e^-$
3. The energy of the electron is 10 GeV and the energy of the proton is 100 GeV. The collider is asymmetric as the energy of colliding particles are different.
4. Convention: forward direction is proton beam direction i.e. positive z axis and backward direction is electron beam direction i.e. negative z axis.
5. Data with high acceptance is used.

6. The selection procedure is done according to the detector acceptance i.e. pseudorapidity (η) $< \mid 3 \mid$, transverse momentum (p_T) $> 0.1\ GeV/c$ and for electron, polar angle (θ) < 2.9 radian ($171.8°$).

3.2 Analysis & Results

The X(3872) decays to $\pi^+\pi^- J/\psi$ which further decays to $\pi^+\pi^-$e$^-$e$^+$ in which J/ψ decays to e^-e^+. So, there are four decay particles electrons (e^-), positrons (e^+), positively charged pions (π^+) and negatively charged pions (π^-). The analysis is done only for electrons and positively charged pions. The positrons and negatively charged pions should have the same distributions as electrons and positively charged pions as they are antiparticles of these particles respectively. Further, in the study, π^+ is referred to as pion.

Each of the figures contains the plots before cuts and after cuts. Here, cuts implies $\mid \eta \mid < 3$, $p_T > 0.1\ GeV/c$.

3.2.1 Pion identification

Study of Kinematic Distributions

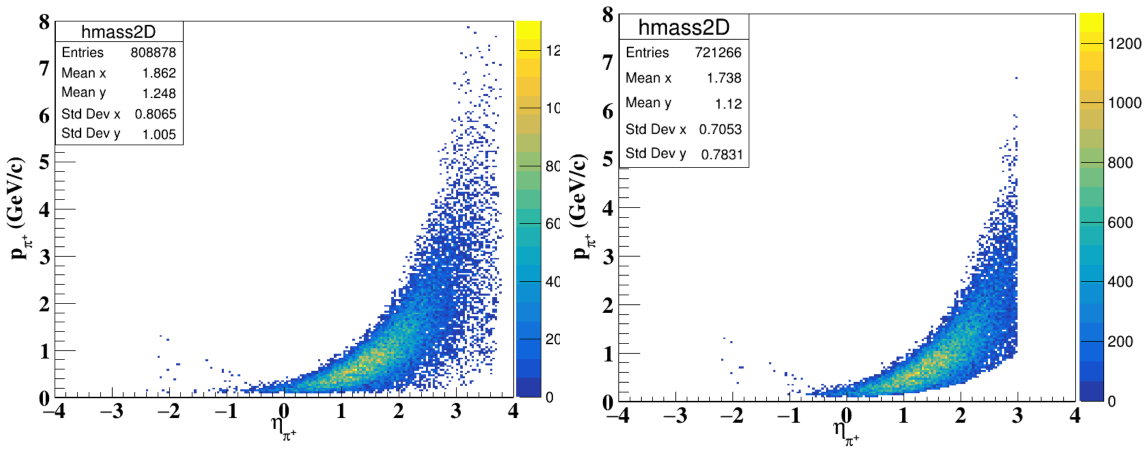

(a) Before cuts

(b) After cuts

Figure 3.1: Momentum versus pseudorapidity distribution of decay pions from X(3872). (a) is before applying cuts and (b) is after applying cuts.

The momentum versus pseudorapidity distribution for decay pions from X(3872) is shown in Figure 3.1. After cuts the pions with higher momentum decreases. Also the momentum range of pions is very less only from 0 to around 8 GeV/c which is expected as pions have less mass as compared to other decay particle of X(3872) that is J/ψ.

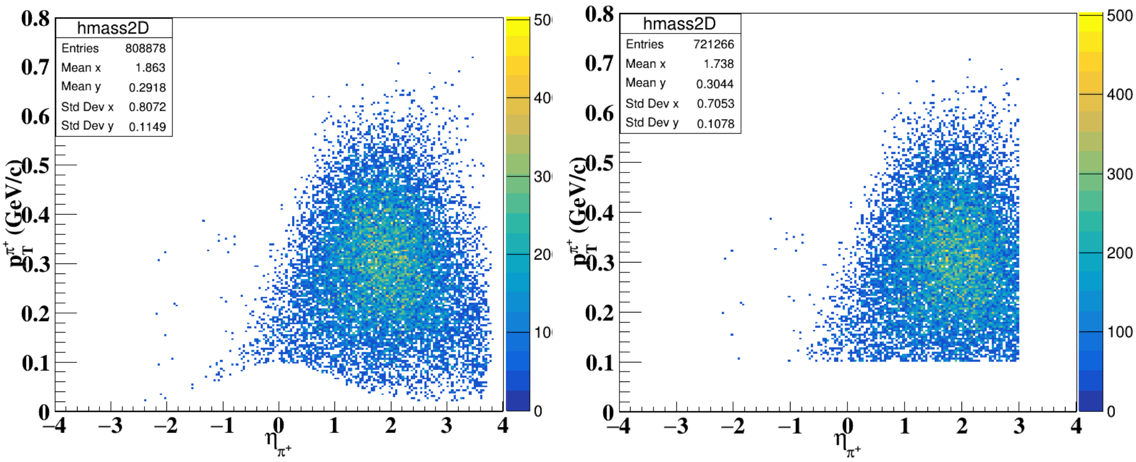

(a) Before cuts

(b) After cuts

Figure 3.2: Transverse momentum versus pseudorapidity distribution for decay pions from X(3872). (a) is before applying cuts and (b) is after applying cuts.

Transverse momentum versus pseudorapidity distribution for decay pions from X(3872) is shown in Figure 3.2. It can be observed that the transverse momentum of pions is very low. A bump around zero is because of the detector's geometry, it can not detect pions in that region.

As seen from both of the distributions, more pions are shifted towards the positive η region which means pions should be detected in the forward region of the detector.

Efficiency of Pion Identification

In Figure 3.3, the upper plot shows the momentum distribution for generated pions, reconstructed pions before cuts, and reconstructed pions after cuts, and the below plot is plotted by taking the ratio of generated and reconstructed pions which is efficiency versus momentum distribution of decay pions from X(3872). It can be seen that the efficiency of pions decreases as momentum increases. It can be observed that the efficiency of pions decreases rapidly as the momentum range increases after applying the cuts which mean fewer reconstructed pions are detected with high momentum.

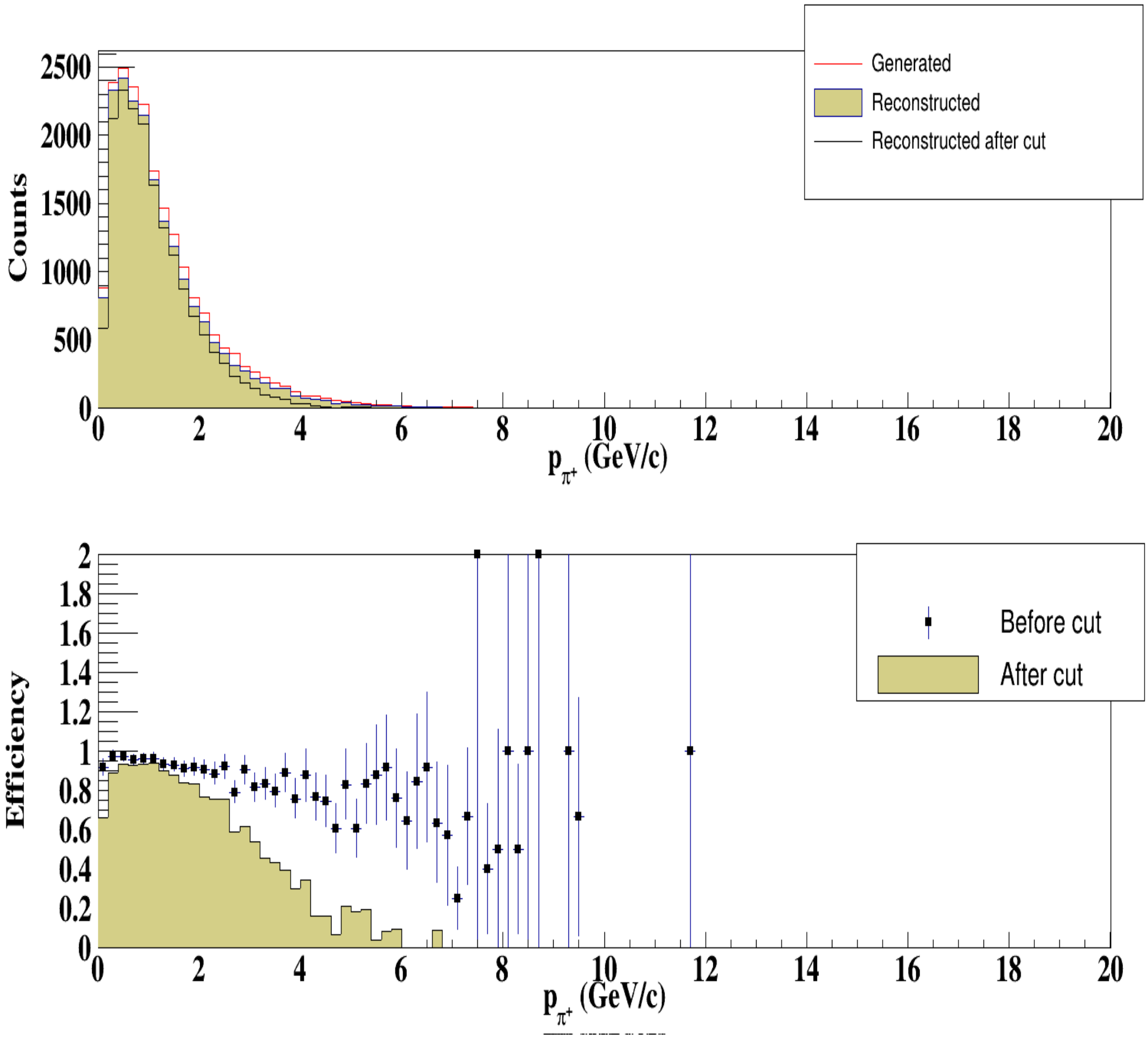

Figure 3.3: The upper plot is a momentum distribution for generated pions(red line), reconstructed pions (shaded) and reconstructed pions after cuts (black line) is shown. The lower plot is an efficiency plot as a function of momentum before cuts (points) and after cuts (shaded) for decay pions.

In Figure 3.4, the upper plot shows the transverse momentum distribution for generated pions, reconstructed pions before cuts, and reconstructed pions after cuts, and the below plot is plotted by taking the ratio of generated and reconstructed pions which is efficiency versus transverse momentum distribution of decay pions from X(3872). It can be observed that the efficiency of pions decreases in the low transverse momentum range before applying the cuts which means the detector is not efficiently detecting pions with low transverse momentum which are removed by applying the cuts. Otherwise, efficiency is almost constant around the value 0.8-0.9.

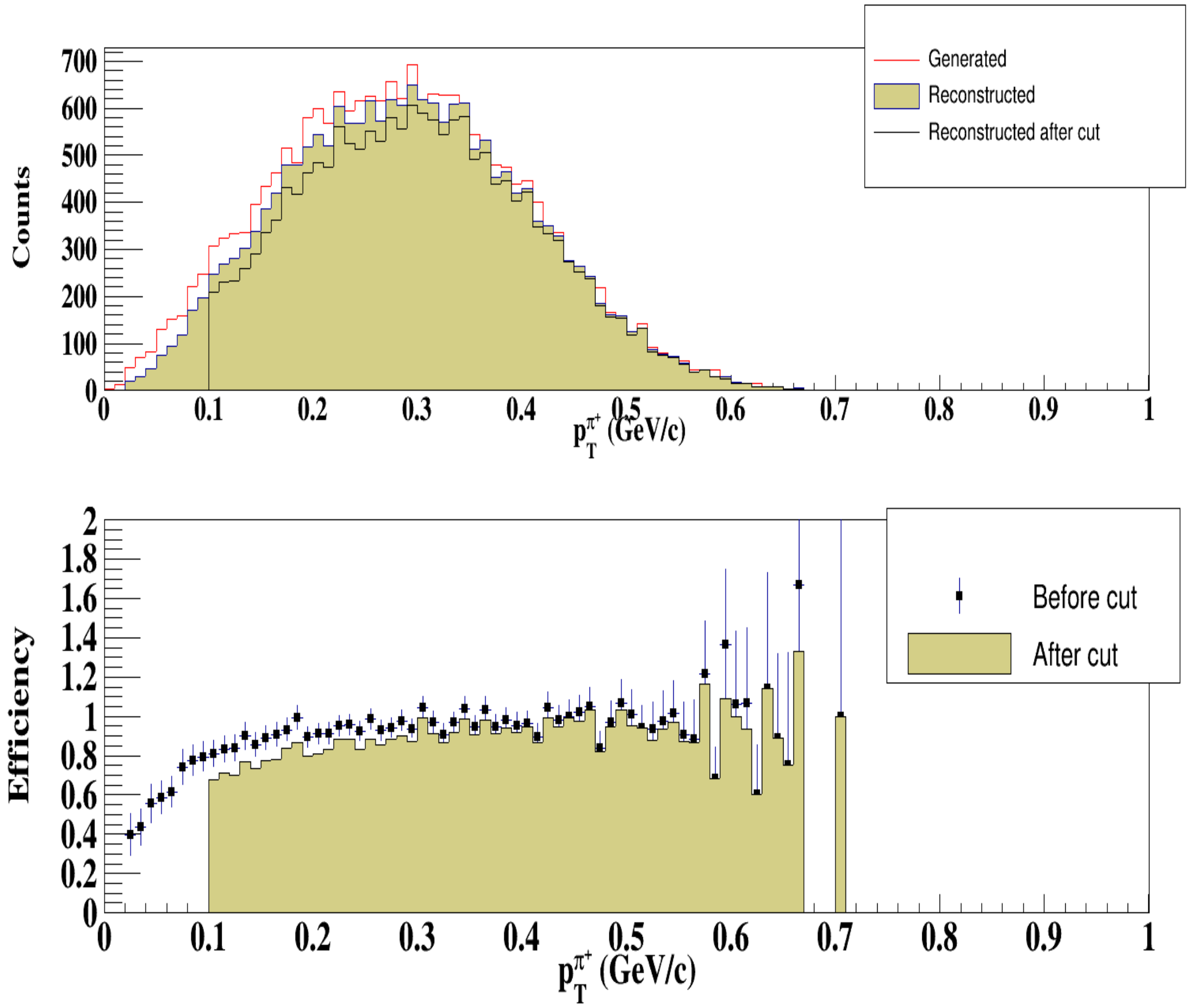

Figure 3.4: The upper plot is a transverse momentum distribution for generated pions (red line), reconstructed pions (shaded), and reconstructed pions after cuts (black line) are shown. The lower plot is an efficiency plot as a function of transverse momentum before cuts (points) and after cuts (shaded).

In Figure 3.5, the upper plot shows the pseudorapidity distribution for generated pions, reconstructed pions before cuts, and reconstructed pions after cuts, and the below plot is plotted by taking the ratio of generated and reconstructed pions which is the efficiency versus pseudorapidity distribution of decay pions from X(3872). It can be observed that the efficiency of pions is near to 1 in around 0-3 η range but decreases to around 0.8 after $\eta = 3$ which is expected that is why cuts are applied for η range.

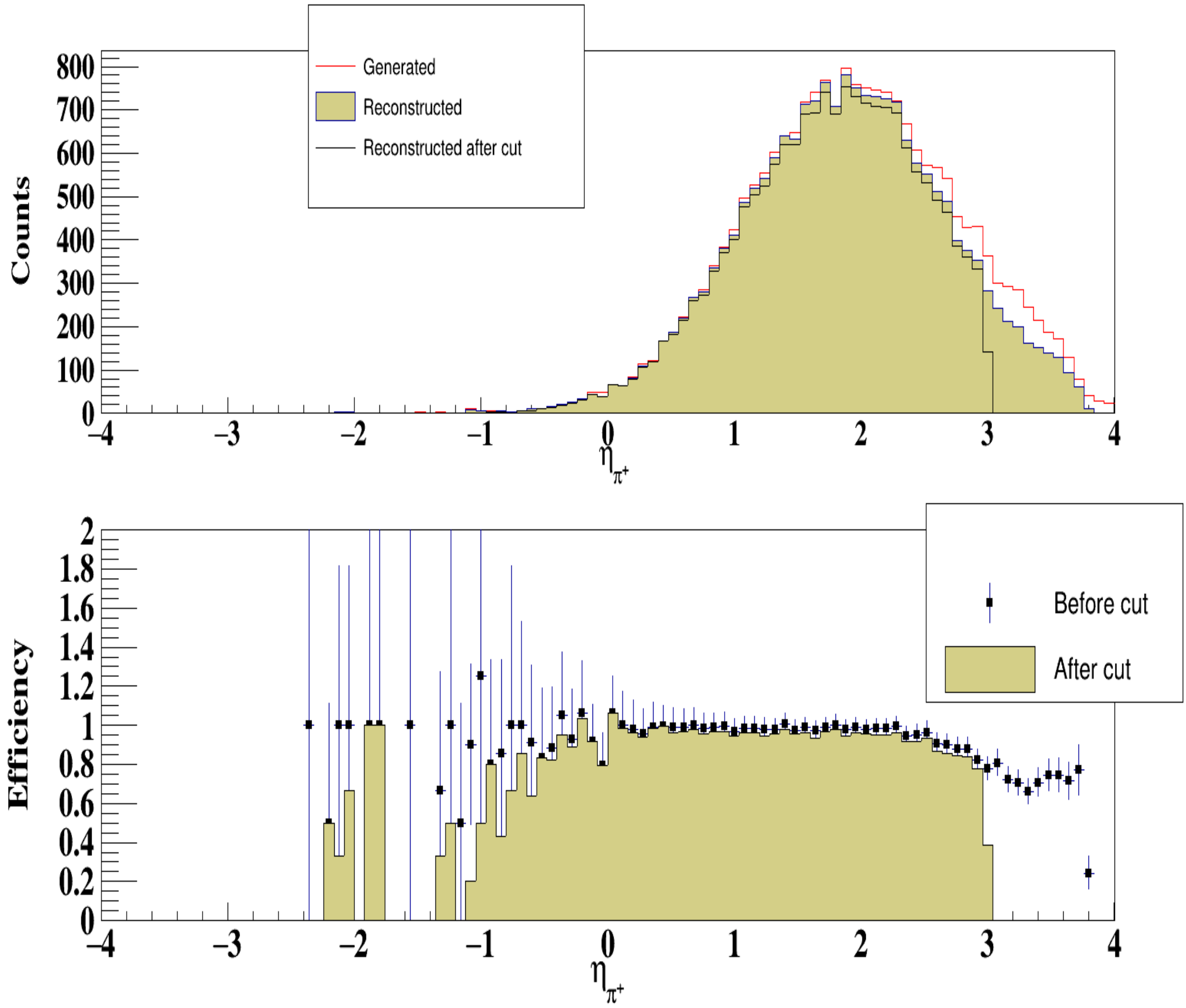

Figure 3.5: The upper plot is pseudorapidity distribution for generated pions (red line), reconstructed pions (shaded) and reconstructed pions after cuts (black line) is shown. The lower plot is an efficiency plot as a function of pseudorapidity before cuts (points) and after cuts (shaded).

3.2.2 Electron identification

Study of Kinematic Distributions

The momentum versus pseudorapidity distribution for decay electrons from X(3872) is shown in Figure 3.6. The cuts does not affect the electron that much. By comparing 3.1 and 3.6, it can be observed that momentum of electrons is much higher than the pions which is obvious because electron is obtained from J/ψ which is having 3.1 GeV/c^2 mass which is very large in comparison to mass of e^-e^+ that is around 1 MeV/c^2, so while decaying the extra mass of J/ψ is converted into kinetic energy of decay electrons leads to high momentum of the electrons.

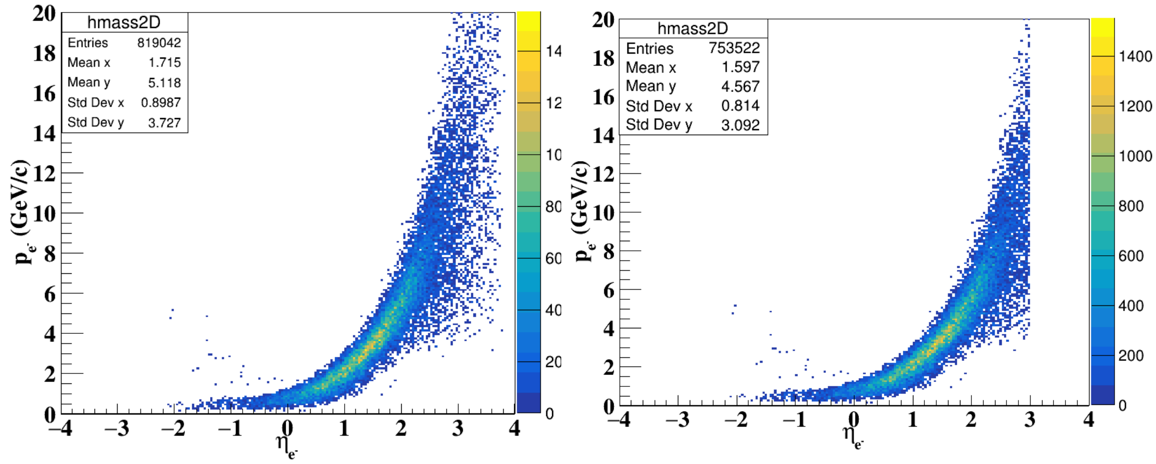

(a) Before cuts (b) After cuts

Figure 3.6: Momentum versus pseudorapidity distribution of decay electrons from X(3872). (a) is before applying cuts and (b) is after applying cuts.

Transverse momentum versus pseudorapidity distribution for decay electrons from X(3872) is shown in Figure 3.7. It can be observed that the transverse momentum of electrons is higher than pions. A curve in 1-3 η range shows detector's limitation that it can not detect electrons in that region.

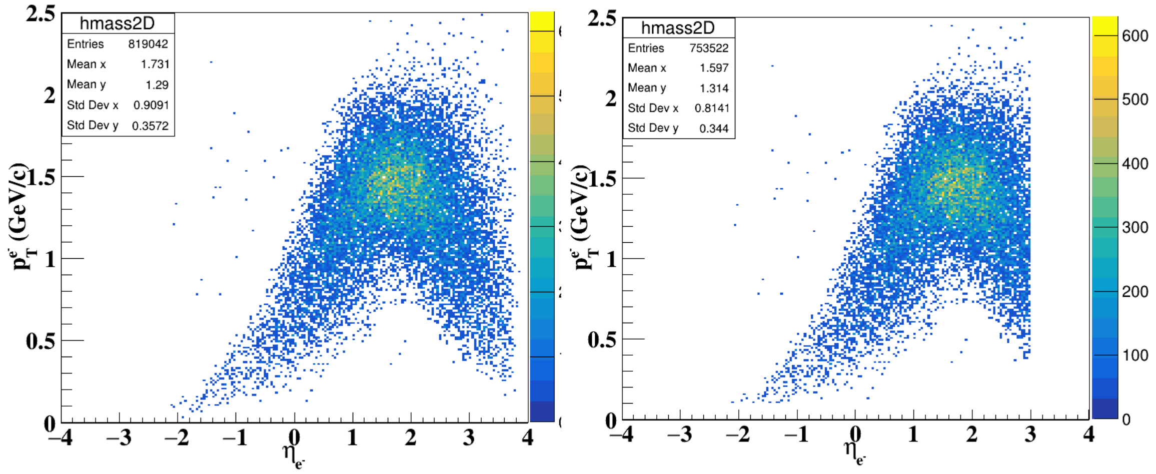

(a) Before cuts (b) After cuts

Figure 3.7: Transverse momentum versus pseudorapidity distribution for decay electrons from X(3872). (a) is before applying cuts and (b) is after applying cuts.

As seen from both of the distributions, more electrons are shifted towards the positive η region which means electrons should be detected in the forward region of the detector.

Efficiency of Electron Identification

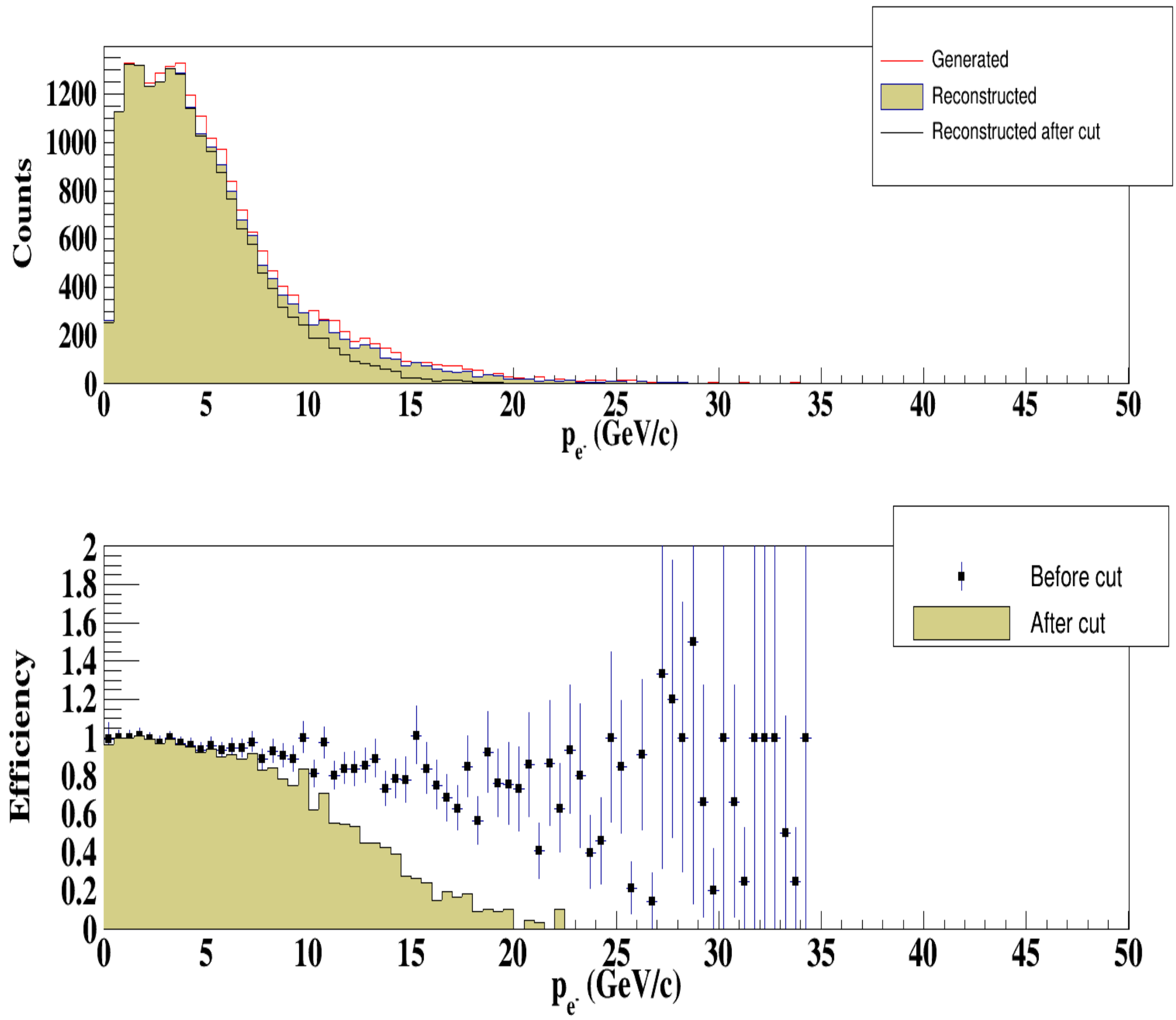

Figure 3.8: The upper plot is a momentum distribution for generated electrons(red line), reconstructed electrons (shaded) and reconstructed electrons after cuts (black line) is shown. The lower plot is an efficiency plot as a function of momentum before cuts (points) and after cuts (shaded).

In Figure 3.8, the upper plot shows the momentum distribution for generated electrons, reconstructed electrons before cuts, and reconstructed electrons after cuts, and the below plot is plotted by taking the ratio of generated and reconstructed electrons which is the efficiency versus momentum distribution of decay electrons from X(3872). It can be seen that the efficiency of electrons decreases as momentum increases. It can be observed that the efficiency of electrons decreases rapidly as the momentum range increases after applying the cuts which means fewer reconstructed electrons are detected with high momentum.

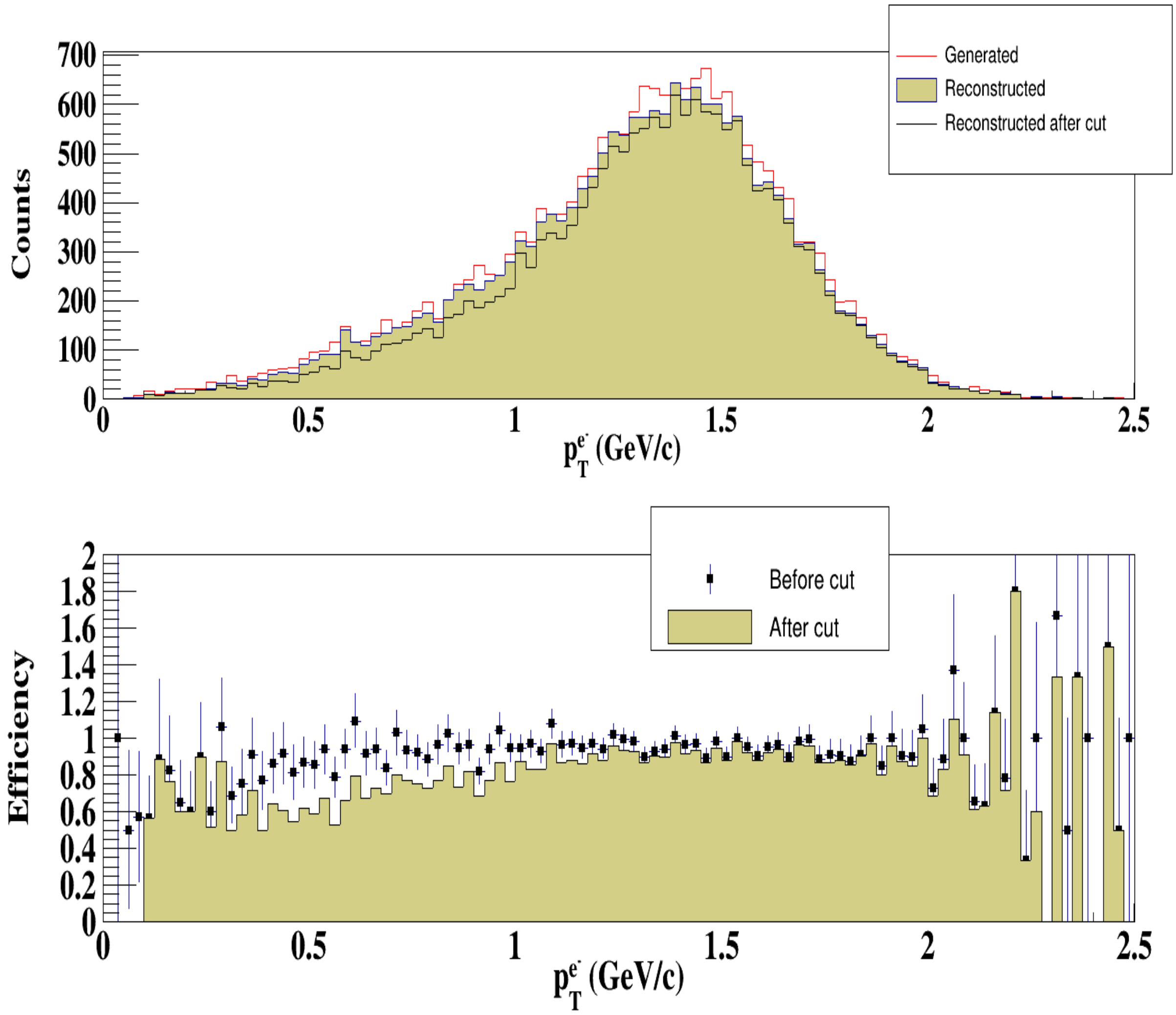

Figure 3.9: The upper plot is a transverse momentum distribution for generated electrons (red line), reconstructed electrons (shaded) and reconstructed electrons after cuts (black line) is shown. The lower plot is an efficiency plot as a function of transverse momentum before cuts (points) and after cuts (shaded).

In Figure 3.9, the upper plot shows the transverse momentum distribution for generated electrons, reconstructuted electrons before cuts and reconstructed electrons after cuts and below plot is plotted by taking ratio of generated and reconstructed electrons which is efficiency versus transverse momentum distribution of decay electrons from X(3872). It can be observed that efficiency of electrons is almost constant near to 1 around 0.5 - 2 (GeV/c) p_T range but decreases to 0.4 in low p_T range.

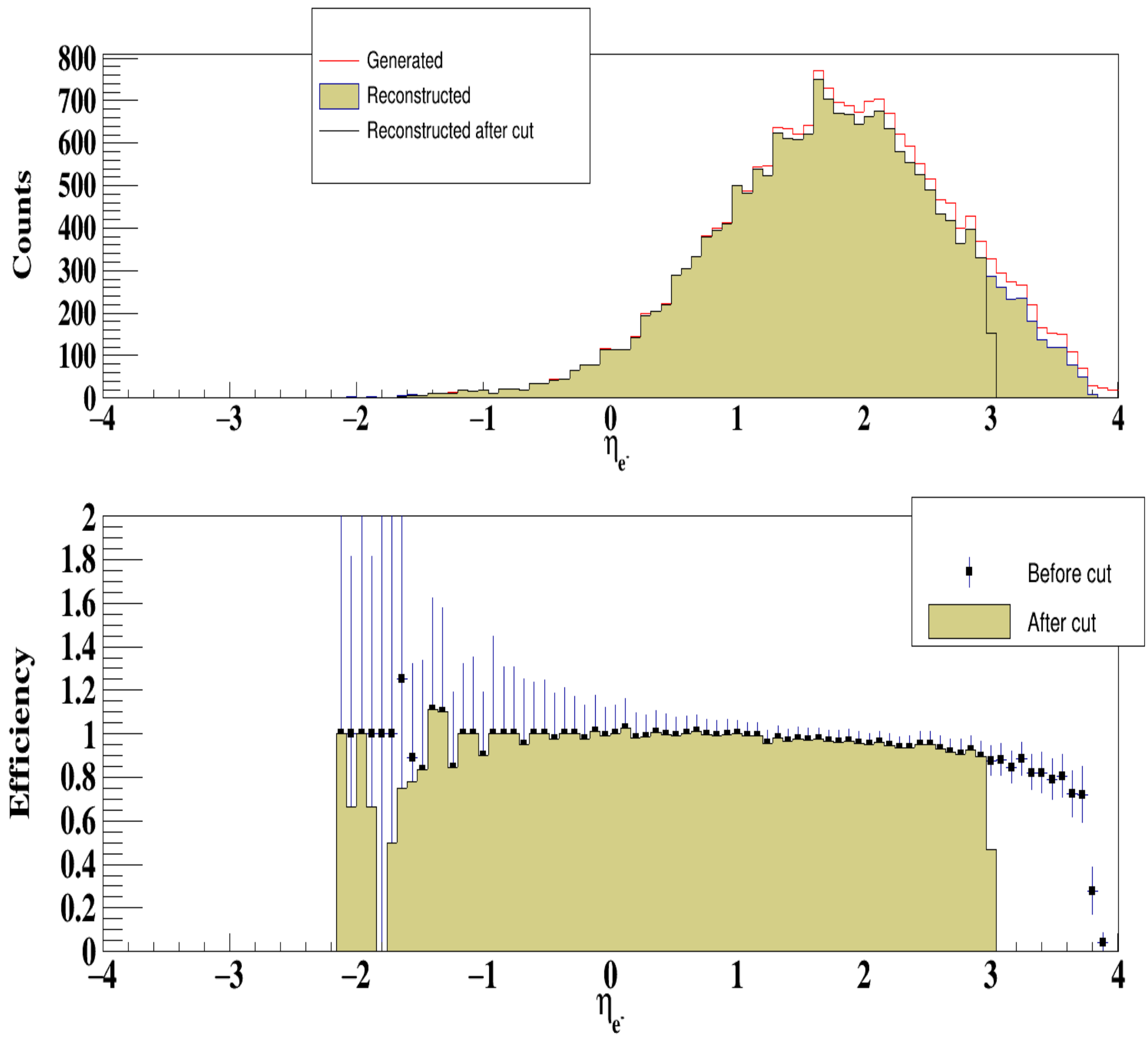

Figure 3.10: The upper plot is pseudorapidity distribution for generated electrons (red line), reconstructed electrons (shaded) and reconstructed electrons after cuts (black line) is shown. The lower plot is an efficiency plot as a function of pseudorapidity before cuts (points) and after cuts (shaded).

In Figure 3.10, the upper plot shows the pseudorapidity distribution for generated electrons, reconstructed electrons before cuts, and reconstructed electrons after cuts, and the below plot is plotted by taking the ratio of generated and reconstructed electrons which is efficiency versus pseudorapidity distribution of decay electrons from X(3872). It can be observed that the efficiency of electrons is near 1 upto $\eta = 3$ but decreases after it which is expected that is why cut is applied for η range.

3.2.3 Mass Resolution for $J/\psi \to e^- e^+$

The mass resolution of J/ψ after applying cuts is shown in Figure 3.11. As shown in the figure, the mean and standard deviation (sigma) for the first Gaussian fitting are -0.00284713 and 0.0187953 and for the second Gaussian fitting are -0.0245476 and 0.0613975. The value of mean and sigma of the curve are -0.01024 and 0.04131, respectively which are very close to zero which is expected. The fitted parameters are computed by ROOT itself. From the χ^2/Ndf test, the goodness of fitting can be known. For this curve χ^2/Ndf value is 2.65 which shows good fitting. Hence, it can be said that J/ψ can be reconstructed very well in the process.

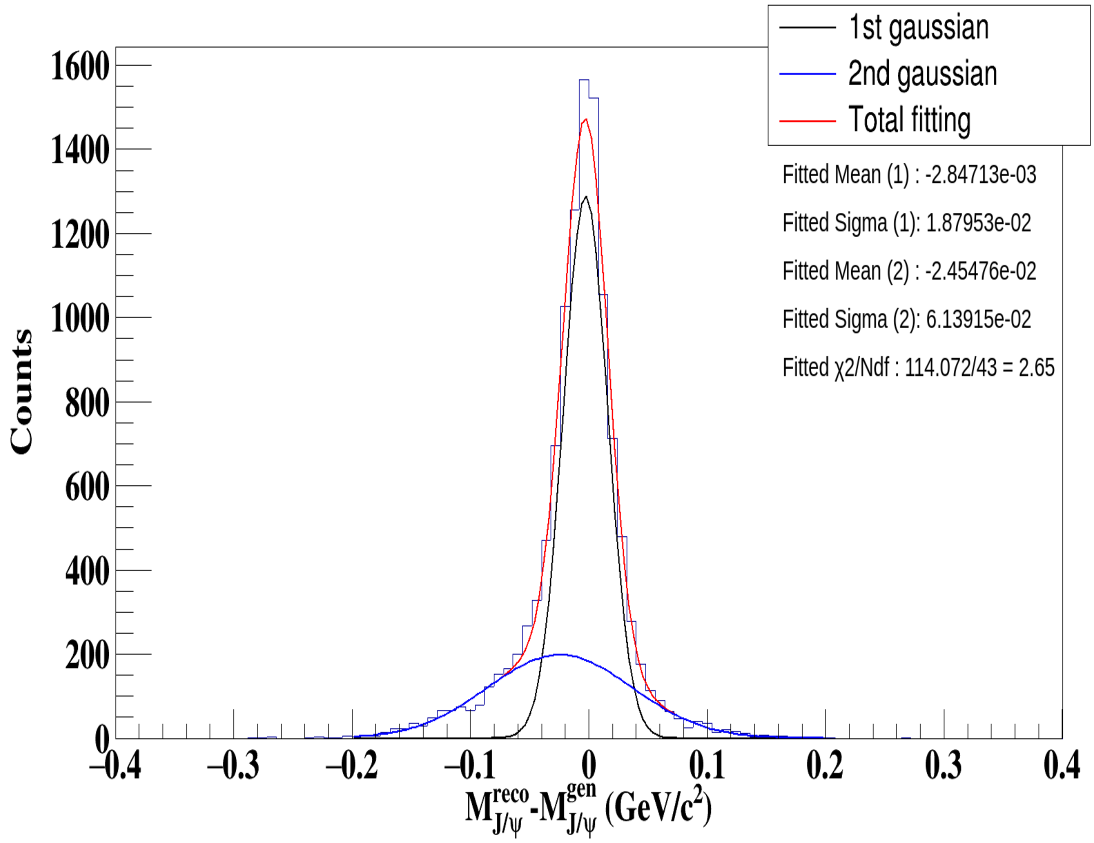

Figure 3.11: Mass resolution of $J/\psi \to e^- e^+$ is plotted after applying cuts. The distribution is fitted with double Gaussian function and here first Gaussian (black line), second Gaussian (blue line) and total (red line) are shown.

3.2.4 Mass Resolution for $X(3872) \rightarrow \pi^+\pi^- J/\psi$

The mass resolution of $X(3872) \rightarrow \pi^+\pi^- J/\psi$ after applying cuts is shown in Figure 3.12. As shown in figure, the mean and standard deviation (sigma) for first Gaussian fitting are -0.00350379 and 0.0201606 and for second Gaussian fitting are -0.0238101 and 0.0626383. The value of mean and sigma of the curve are -0.01073 and 0.04254, respectively which are very close to zero which is expected. For this curve χ^2/Ndf value is 2.11 which shows good fitting. Hence, it can be said that X(3872) can be reconstructed very well in the process.

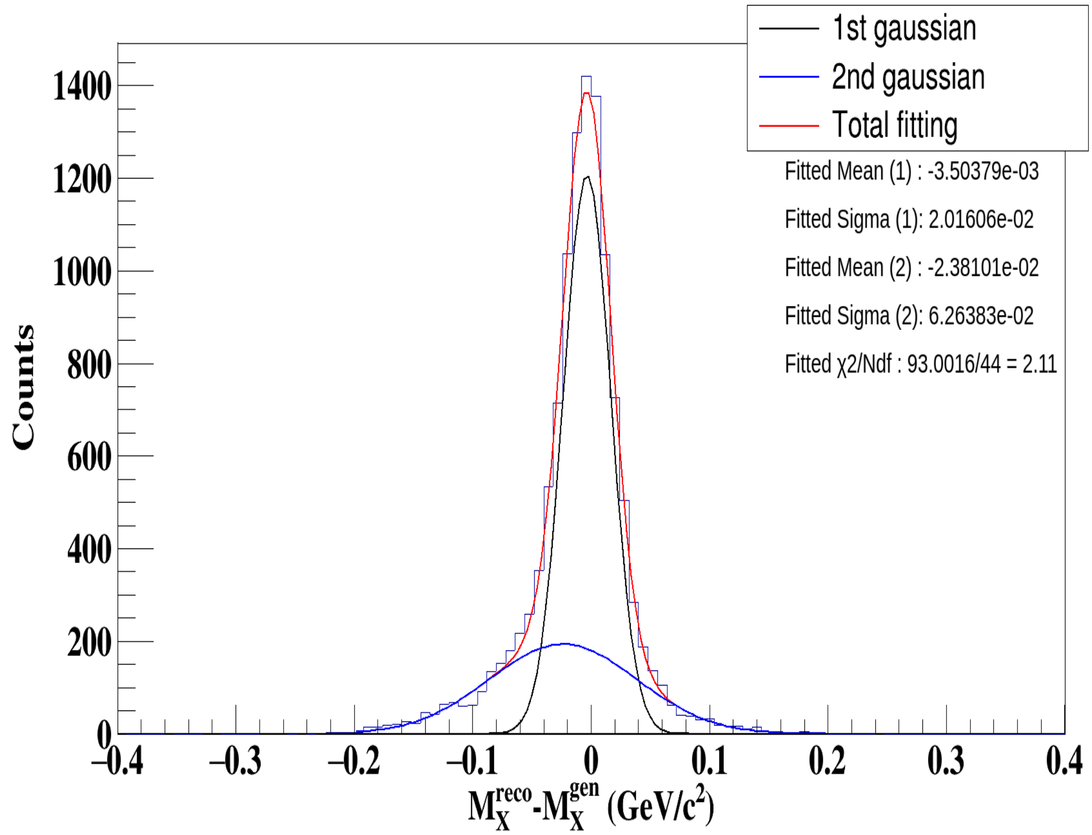

Figure 3.12: Mass resolution of $X(3872) \rightarrow \pi^+\pi^- J/\psi$ is plotted after applying cuts. The distribution is fitted with double Gaussian function and here first Gaussian (black line), second Gaussian (blue line) and total (red line) are shown.

3.2.5 Mass Difference for J/ψ vs Kinematic Variables for e$^-$

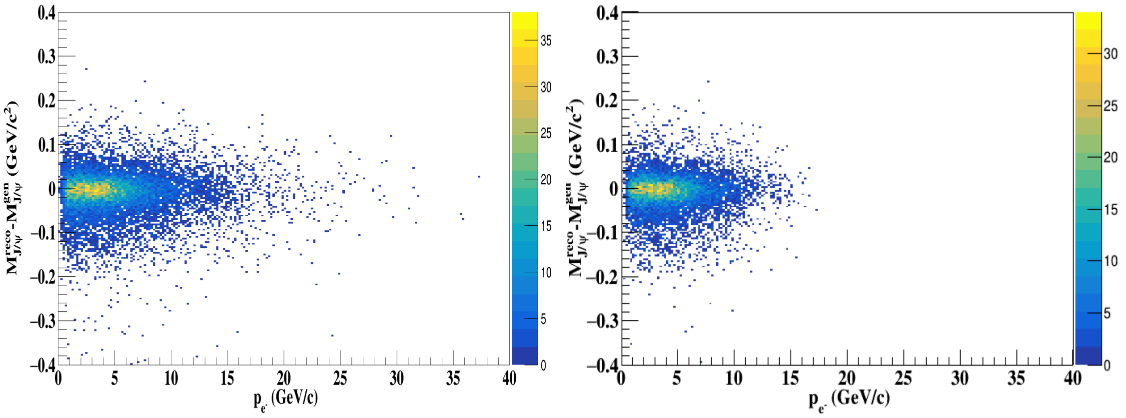

(a) Before cuts (b) After cuts

Figure 3.13: Mass Difference of J/$\psi \to$ e$^-$e$^+$ versus momentum of electron decay from X(3872) is plotted. Here (a) is obtained before applying cuts and (b) is obtained after applying cuts.

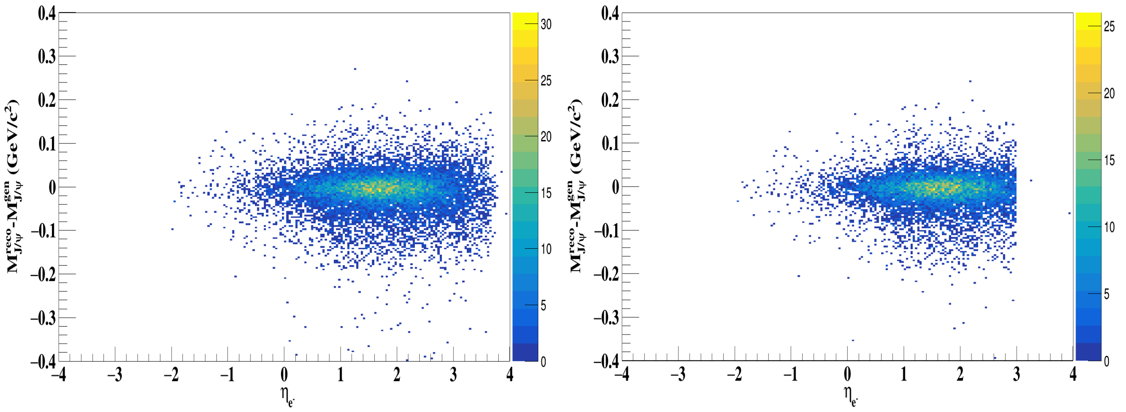

(a) Before cuts (b) After cuts

Figure 3.14: Mass Difference of J/$\psi \to$ e$^-$e$^+$ versus pseudorapidity of electrons is plotted. Here (a) is obtained before applying cuts and (b) is obtained after applying cuts.

The mass difference of J/ψ versus momentum and pseudorapidity of J/ψ decay electrons are shown in Figure 3.13 and 3.14, respectively. We are looking for how the mass difference is distributed over the entire η range and p range. We are focussing on the mass difference because it is the quantity that can tell us how precise our measurements are. If the value of the mass difference is zero or near zero then we can say that the measurements are good enough. So, by looking at the entire η or p range, we are searching in which region the spread of mass difference is less.
The conclusion of this study is given in the conclusion and outlook section.

Chapter 4

Structure of Exotic Particle X(3872)

The exotic particles can have different structures and here the structure of exotic particle X(3872) is explored. The possible structure of X(3872) is either molecular or compact tetraquark. To know its structure AMPT model is used which is designed for heavy ion collisions which produce the QGP medium. In the QGP medium, the different structures behave differently which can help to know the structure of X(3872). AMPT by default does not generate X(3872) but it can generate D mesons and as it was known that X(3872) can be made by coalescence of two D mesons. In this chapter, we are studying the molecular nature of the X(3872) using AMPT.

4.1 Deciphering Nature of X(3872)

The collision of two heavy nuclei like Pb-Pb or Au-Au at relativistic energies makes it viable to look into the nuclear matter. Quark-Gluon Plasma (QGP) which is produced in relativistic heavy ion collisions is defined as a (locally) thermally equilibrated state of matter in which quarks and gluons are deconfined from hadrons so that they propagate over nuclear, rather than merely nucleonic, volumes. So, in relativistic heavy ion collisions, a new state of matter (QGP) can be created at temperatures of more than 10^8 times the surface temperature of the Sun, the hottest matter created in the lab to date. Relativistic heavy ion collision can be a good experiment to study the structure of exotic particles because it produces the QGP medium. Different natures of exotic particles will behave differently in the QGP medium helps in knowing the natures of exotic particles.
The CMS Collaboration [12] announced the first experimental evidence of X(3872) in Pb-Pb collisions at the Large Hadron Collider (LHC, making an important first

step toward the investigation of exotic particles in heavy ion collisions.
The structure of X(3872) is studied using heavy ion collision through an AMPT event generator which will implement the production mechanism for its possible molecular structure.

4.2 AMPT Framework

For study a string melting version of AMPT is used at $\sqrt{s} = 2.76$ TeV for generating data by varying some of the parameters in 'input.ampt'. Some of the parameters did not change during the whole study. The parameters changed are:

1. Center of mass energy: EFRM = 2760 GeV.

2. Atomic mass of the projectile and target nucleus: IAP and IAT = 208 for Pb.

3. Atomic number of the projectile and target nucleus: IZP and IZT = 82 for Pb.

4. Number of events: NEVNT (vary according to need).

5. Maximum and minimum value of impact parameter (transverse distance between the center of mass of two nuclei which is 0 for central collisions and maximum for ultraperipheral collisions): BMIN and BMAX = 2.5 (0-10% centrality), 9.8 (30-50% centrality) [13].

6. Value for choosing default or string melting version of AMPT: ISOFT = 4 for string melting.

7. Lund string fragmentation parameters a and b: PARJ(41) and PARJ(42), the value of parton screening mass and value of alpha in parton cascade (vary according to need).

The D mesons like D^0, D^+ and D^{*+} are charmed mesons. Detailed information about D mesons is given in Table 4.1 [14].

Table 4.1: D mesons.

Particle (antiparticle)	Quark Composition	Mass (MeV/c^2)
D^+ (D^-)	$c\bar{d}$	1869.62±0.20
D^0 ($\bar{D}^0$)	$c\bar{u}$	1864.84±0.17
D_s^+ (D_s^-)	$c\bar{s}$	1968.47±0.33
D^{*+} (D^{*-})	$c\bar{d}$	2010.27±0.17
D^{*0} ($\bar{D}^{*0}$)	$c\bar{u}$	2006.97±0.19

It is known that the molecular structure of X(3872) can be made by the coalescence of two charmed mesons. So, by measuring the observables for D mesons, the behavior of D mesons can give an idea about the molecular X(3872) state. In simulations, molecular X(3872) is formed by coalescence of two D mesons with constraints: 5 fm < relative distance < 7 fm and $2M_D$ < pair mass < $2M_D{}^*$.
In search for the molecular state of X(3872), transverse momentum, rapidity, and elliptic flow (v_2) vs transverse momentum distribution for D^0, D^+ and D^{+*} is plotted to know the behavior if it matches with some experimental results.
The AMPT program that is available for us is not designed for heavy flavors and also charm production is statistically poor which is a problem for this work. The D mesons production in our simulations is very less. Number of D^{+*} and D^{0*} is very less compared to D^+ and D^0. D mesons are identified using particle identification (PIDs) numbers which is 421 for D^0, 411 for D^+, and 413 for D^{+*}.

4.3 Analysis & Results

4.3.1 Study of D Mesons

The transverse momentum and rapidity distributions for 0% - 10% centrality and elliptic flow coefficient ($\mathrm{v_2}$) vs transverse momentum distribution for 30% - 50% centrality is plotted. 30% - 50% centrality is taken for elliptic flow because space momentum anisotropy is best visible in peripheral collisions (value of impact parameter is between 0 and twice the radius of nucleus). Around 50,000 events are generated in Pb-Pb collision using AMPT event generator at $\sqrt{\mathrm{s}} = 2.76$ TeV.
Figure 4.1 shows transverse momentum spectra of D^0, D^+ and D^{*+} in Pb-Pb collision with $-0.5 < y < 0.5$ cut. It shows overall same trend as normal hadrons for D^0, D^+ but the slope is harder at higher $\mathrm{p_T}$ for D^{*+}. This is because our AMPT is not designed for heavy flavor. As D^{*+} has higher mass than D^0, D^+, its production in our simulation get affected.
Figure 4.2 shows rapidity distribution of D^0, D^+ and D^{*+} in Pb-Pb collision. It shows same trend as normal hadrons being flat in mid rapidity region and decreasing towards forward and backward direction.
The elliptic flow coefficient vs transverse momentum distribution is shown in Figure 4.3. The D^0 and D^+ first increases and then decreases as p_T range increases which is expected but D^{*+} show opposite trend as it first decreases then increases with increasing p_T range.

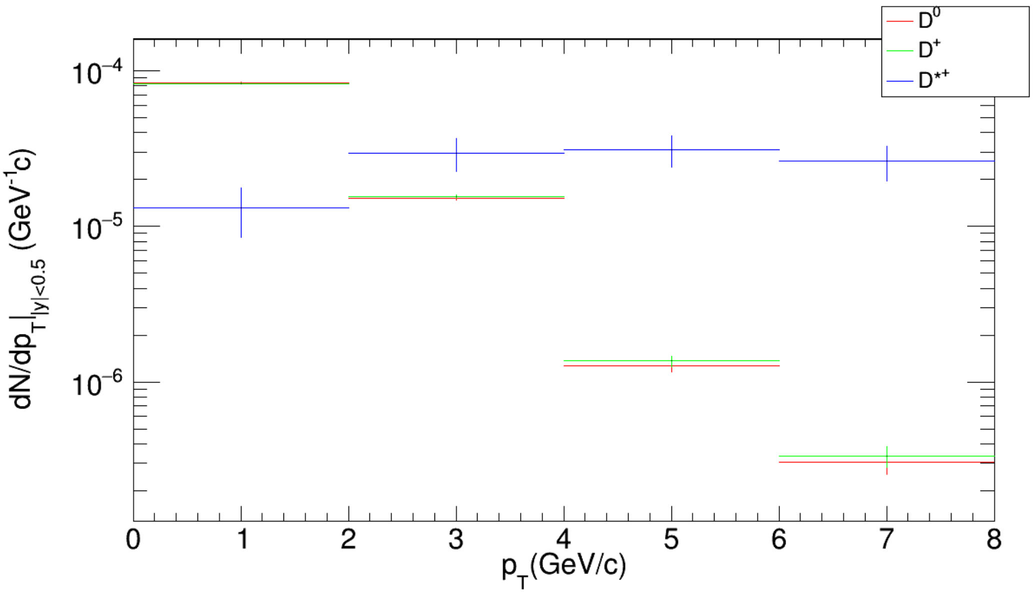

Figure 4.1: Transverse momentum spectra of D^0 (red line), D^+ (green line) and D^{*+} (blue line) computed from simulations within rapidity range of ± 0.5.

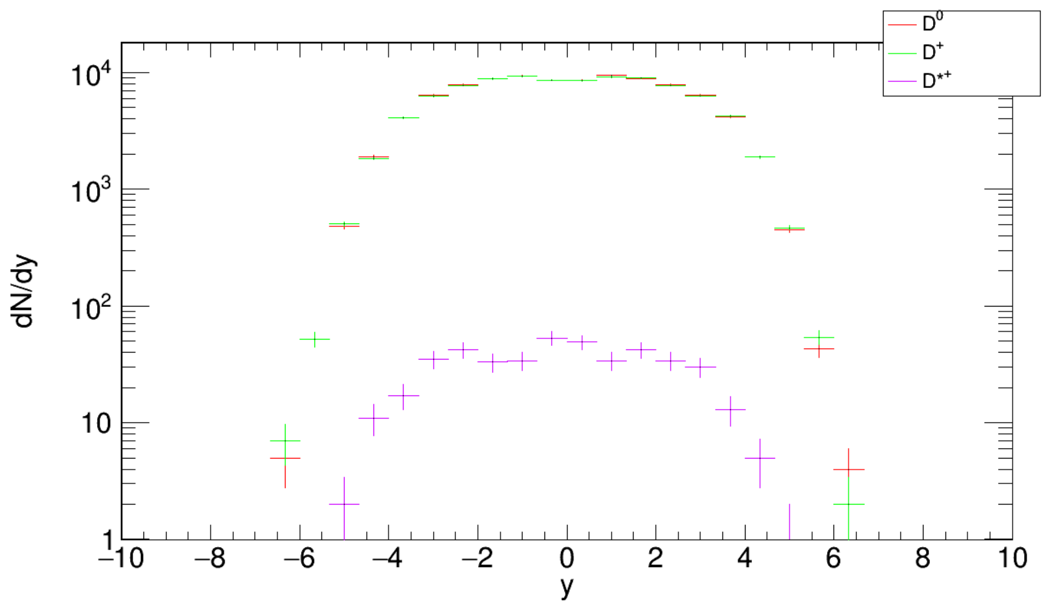

Figure 4.2: Rapidity spectra of D^0 (red line), D^+ (green line) and D^{*+} (violet line) computed from simulations.

The comparison of transverse momentum distribution for simulated data generated in Pb-Pb collision with ALICE data for D^0 and D^+ as shown in Figure 4.5. It can be observed that in the low p_T region AMPT can explain ALICE results [15], however, it fails for the high p_T region.

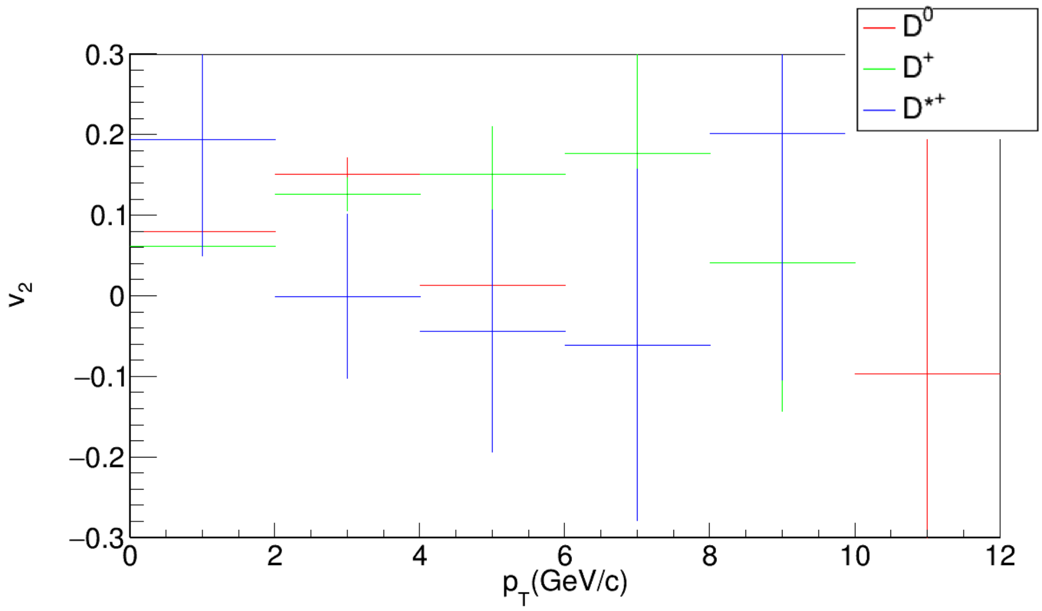

Figure 4.3: The elliptic flow coefficient vs transverse momentum distribution in $-0.8 < y < 0.8$ of D^0 (red line), D^+ (green line) and D^{*+} (blue line) computed from simulations.

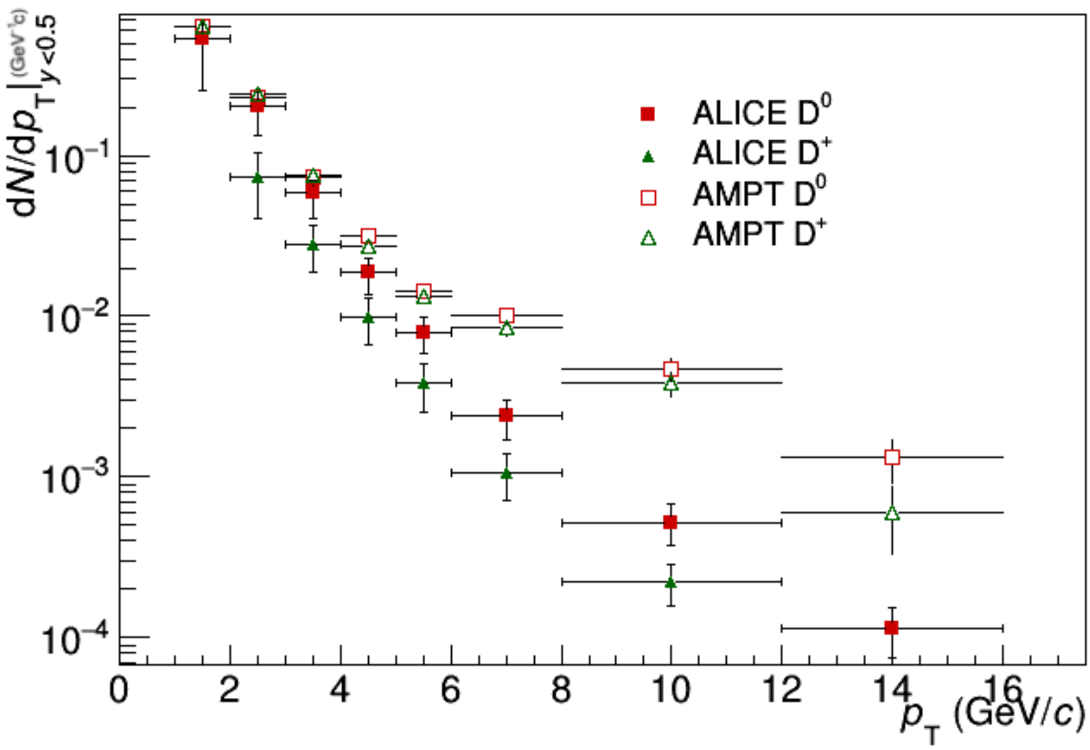

Figure 4.4: Transverse momentum distribution of simulated data for D^0 (empty red square) and D^+ (empty green triangle) in Pb-Pb collision. This result is compared with ALICE data for D^0 (filled red square) and D^+ (filled green triangle).

4.3.2 Molecular X(3872)

The mass threshold of X(3872) lies near to $D\bar{D}^*$ or its charge conjugate. But in simulations, it is difficult to get D^* or its charge conjugate. As X(3872) contains a charm-anticharm pair, D^+ and its charge conjugate $\bar{D^+}$ is used to make molecular X(3872). The mass threshold of $D^+\bar{D^+}$ is around 132.76 MeV lower than the threshold of X(3872). In one of the experiments [16], the invariant mass distribution of X(3872) as $D\bar{D}$ is studied. So, this combination $D^+\bar{D^+}$ can be taken for molecular X(3872).
Around 218000 events in Pb-Pb collision are generated at $\sqrt{s} = 2.76$ TeV from which after coalescence only 88 molecular X(3872) are generated. For coalescence ΔP that is momentum difference of coalescencing D^+ and $\bar{D}^+$ is taken 0.2 GeV/c and ΔR that is coordinator distance between D^+ and $\bar{D}^+$ is taken 6 fm. Transverse momentum distribution of generated X(3872) from simulations is plotted as shown in Figure 4.5. It shows similar trend as normal hadrons, decreasing towards high p_T range. Also, it follows same trend as X(3872) formed using updated AMPT which is heavy flavor designed.

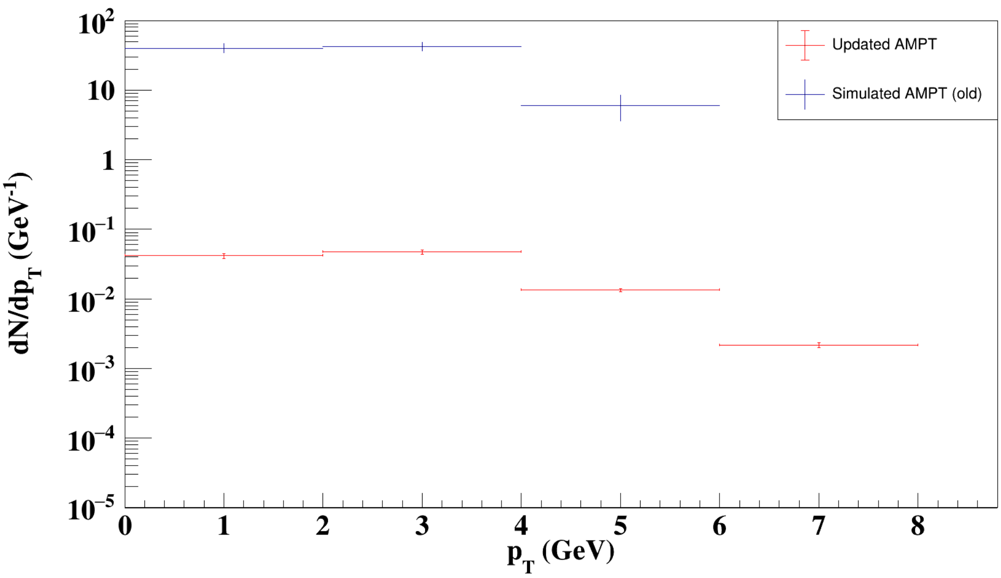

Figure 4.5: Transverse momentum distribution of simulated data for X(3872) molecular structure in Pb-Pb collision. Comparison of simulated data (blue line) and data generated from updated version of AMPT model [6] (red line).

The conclusion of this study is given in conclusion and outlook section.

Conclusion & Outlook

The feasibility study of X(3872) was discussed in chapter 3. X(3872) was found with very low background. Different kinematics distributions of X(3872) decay leptons and pions like momentum versus pseudorapidity, and transverse momentum vs pseudorapidity were studied. From the kinematics distribution, it was found that decay particles of X(3872) lie in the backward direction. The reconstruction efficiency of decay leptons and pions from X(3872) was studied. It. The mass resolution of J/ψ and X(3872) was studied. It can be concluded that it is very much possible to identify X(3872) in the EIC experiment. The mass difference (reconstructed mass-generated mass) of J/ψ versus momentum and pseudorapidity were also discussed.

So, it can be said that X(3872) should be produced for 10-100 GeV electron-proton collision in future EIC. In the future, a similar study can be done in electron nucleus collision. Also, study X(3872) with different background can be done in future EIC experiment.

The D mesons and X(3872) are studied in heavy ion collision that is Pb-Pb at the center of mass energy $\sqrt{s}$ = 2.76 TeV. As the AMPT model accessible to us is not heavy flavor designed, there is difficulty in the production of D^* or its charge conjugate. Different distributions like transverse momentum, rapidity, and elliptic flow vs transverse momentum distribution are studied for D^0, D^+, and D^*, and a problem is found in the production of D^*. A comparison of the transverse momentum distribution of simulated data for D^0 and D^+ with experimental ALICE data for the same is done. At last, by coalescence of D^+ and $\bar{D^+}$, the molecular state was tried to be formed and studied the transverse momentum distribution. But the statistics obtained in updated AMPT is quite high in comparison to simulated data obtained in this study. So, anything about the molecular case is not predicted for now from this study.

In the future, further coalescence of D and D^* to match the exact threshold can be done. The study of the tetraquark nature of X(3872) can be done in the future. As the updated version of AMPT is not publically accessible till now, in the future if we get it we can get better results.

Glossary

AMPT	A Multiphase Transport Model
ATHENA	A Totally Hermetic Electron Nucleus Apparatus
bECal	barrel Electromagnetic Calorimeter
bHCal	barrel Hadron Calorimeter
DIRC	Detection of Internally Reflected Cherenkov light
dRICH	dual-radiator RICH
EIC	ELectron Ion Collider
GEM	Gas Electron Multiplier
hpDIRC	high-performance DIRC
IP6	Interaction Point 6
nECal	electron-endcap Electromagnetic Calorimeter
nHCal	electron-endcap Hadron Calorimeter
pECal	hadron-endcap Electromagnetic Calorimeter
pfRICH	proximity-focusing RICH
pHCal	hadron-endcap Hadron Calorimeter
PID	Particle Identification
QCD	Quantum Chromodynamics
QGP	Quark Gluon Plasma
RICH	Ring Imaging Cherenkov
ToF	Time-of-Flight

References

1. David J Griffiths. Introduction to elementary particles; 2nd rev. version. Physics textbook. Wiley, New York, NY, 2008.

2. Nora Brambilla, Simon Eidelman, Christoph Hanhart, Alexey Nefediev, Cheng-Ping Shen, Christo-pher E. Thomas, Antonio Vairo, and Chang-Zheng Yuan. The XYZ states: Experimental and theoretical status and perspectives. Physics Reports, 873:1–154, Aug 2020.

3. S. K. Choi et al. (Belle Collaboration), Phys. Rev. Lett. 91, 262001 (2003).

4. Science requirements and detector concepts for the electron-ion collider: Eic yellow report, 2021.

5. R . Aaij, et al., Determination of the X(3872) meson quantum numbers, Phys. Rev. Lett. 110 (2013) 222001. arXiv:1302.6269, doi:10.1103/PhysRevLett.110.222001.

6. Hui Zhang, Jinfeng Liao, Enke Wang, Qian Wang, and Hongxi Xing. Deciphering the nature of X(3872) in heavy ion collisions. Physical Review Letters, 126(1), Jan 2021.

7. Kohsuke Yagi, Tetsuo Hatsuda, and Yasuo Miake. Quark-gluon plasma: from big bang to little bang, Cambridge monographs on particle physics, nuclear physics and cosmology.

8. Rene Brun and Fons Rademakers, ROOT - An Object Oriented Data Analysis Framework, preceedings AIHENP'96 workshop , Lausanne , sep. 1996, nucl. inst. & meth. in phys. res. A 389 (1997) 81-86.

9. ATHENA Detector Proposal, ATHENA Collaboration, November 29, 2021.

10. eic.phy.anl.gov/ip6/howto/use_singularity.html

11. Zi-Wei Lin, Che Ming Ko, Bao-An Li, Bin Zhang, and Subrata Pal. Multiphase transport model for relativistic heavy ion collisions. Physical Review C, 72(6), Dec 2005.

12. CMS Collaboration, 2019, http://cds.cern.ch/record/2698963.

13. Centrality determination of Pb–Pb collisions at $\sqrt{s_{NN}}$= 2.76 TeV with ALICE Collaboration. Betty Abelev (LLNL, Livermore) et al. e-Print: 1301.4361 [nucl-ex]. DOI: 10.1103/PhysRevC.88.044909. Phys.Rev.C 88 (2013) 4, 044909

14. The Review of Particle Physics (2021). P.A. Zyla et al. (Particle Data Group), Prog. Theor. Exp. Phys. 2020, 083C01 (2020) and 2021 update.

15. Transverse momentum dependence of D-meson production in Pb-Pb collisions at $\sqrt{s_{NN}}$ = 2.76 TeV. ALICE Collaboration. Jaroslav Adam (Prague, Tech. U.) et al. e-Print: 1509.06888 [nucl-ex] DOI: 10.1007/JHEP03(2016)081. JHEP 03 (2016), 081

16. Belle Collaboration, K. Abe et al., hep-ex/0307061.